https://doi.org/10.5194/se-2019-140
Preprint. Discussion started: 23 September 2019

Solid Earth Discussions

Tracing fluid transfers in subduction zones: an integrated thermodynamic and $\delta^{18}O$ fractionation modelling approach

Alice Vho[1], Pierre Lanari[1], Daniela Rubatto[1,2], Jörg Hermann[1]

[1] Institute of Geological Sciences, University of Bern, CH-3012 Bern, Switzerland
[2] Institut de Sciences de la Terre, University of Lausanne, CH-1015 Lausanne, Switzerland

Correspondence to: Alice Vho (alice.vho@geo.unibe.ch)

Abstract. Oxygen isotope geochemistry is a powerful tool for investigating rocks that interacted with fluids, to assess fluid sources and quantify the conditions of fluid-rock interaction. We present an integrated modelling approach and the computer program PTLOOP that combine thermodynamic and oxygen isotope fractionation modelling for multi-rock open systems. The strategy involves a robust petrological model performing on-the-fly Gibbs energy minimizations coupled to an oxygen fractionation model both based on internally consistent databases. This approach is applied to subduction zone metamorphism to predict the possible range of $\delta^{18}O$ values for stable phases and aqueous fluids at various pressure-temperature (P-T) conditions in the subducting slab. The modelled system is composed by a sequence of oceanic crust (mafic) with sedimentary cover of known initial chemical composition and bulk $\delta^{18}O$. The evolution of mineral assemblage and $\delta^{18}O$ values of each phase is calculated along a defined P-T path. Fluid-rock interactions may occur as consequence of (1) infiltration of an external fluid into the mafic rocks or (2) transfer of the fluid liberated by dehydration reactions occurring in the mafic rocks into the sedimentary rocks. The effects of interaction with externally-derived fluids on the mineral and bulk $\delta^{18}O$ of each rock are quantified for two typical compositions of metabasalts and metasediments with external fluid influx from serpentinite. The dehydration reactions, fluid loss and mineral fractionation produce minor to negligible variations in bulk $\delta^{18}O$ values, i.e. within 1 ‰. By contrast, the interaction with external fluids may lead to shifts in $\delta^{18}O$ up to one order of magnitude larger. Such variations can be detected by analysing in-situ oxygen isotope in key metamorphic minerals such as garnet, white mica and quartz. The simulations show that, when the water released by the slab infiltrates the forearc mantle wedge, it can cause extensive serpentinization within fractions of a Myr and significant oxygen isotope variation at the interface. This technique opens new perspectives to track fluid pathways in subduction zones, to distinguish porous from channelized fluid flows, and to determine the P-T conditions and the extent of fluid/rock interaction.

1 Introduction

The subducting oceanic slab is composed of a sequence of rock types corresponding to chemical systems that undergo continuous and discontinuous phase reaction in response to pressure and temperature changes. Through its metamorphic history, altered oceanic lithosphere undergoes extensive dehydration by the breakdown of low-temperature, volatile rich minerals (e.g., Baumgartner and Valley, 2001; Baxter and Caddick, 2013; Hacker, 2008; Manning, 2004; Page et al., 2013; Poli and Schmidt, 2002). The expelled water migrates through the slab towards the slab-mantle interface and it may continue rising to the mantle wedge playing a major role in triggering mass transfer and melting (Barnicoat and Cartwright, 1995; Bebout and Penniston-Dorland, 2016). Evidence of fluid circulation in subducted rocks has been extensively observed in exhumed high-pressure/ultra-high-pressure (HP/UHP) terrains (e.g., Zack and John, 2007; Baxter and Caddick, 2013; Martin *et al.*, 2014; Rubatto and Angiboust, 2015; Engi *et al.*, 2018), but a direct link to the primary source production is often missing and the main source remains matter of debate. The characterization of fluid pathways in subduction zones has been addressed by using a variety of methods (i.e., seismicity, thermodynamic modelling, fluid inclusions, HP veins, trace element and stable isotope studies on metamorphic minerals) (e.g., Baxter and Caddick, 2013; Hacker, 2008; Hernández-Uribe and Palin, 2019; Scambelluri and

https://doi.org/10.5194/se-2019-140
Preprint. Discussion started: 23 September 2019

Philippot, 2001; Spandler and Hermann, 2005). In particular, oxygen isotope compositions of metamorphic minerals from exhumed HP rocks shed light on the nature of the fluid reacting with those systems during metamorphism. Thus, oxygen isotope studies of HP rocks have the potential to make important contributions to the investigation of fluid sources and pathways in subduction zones (e.g., O'Neil and Taylor, 1967; Muehlenbachs and Clayton, 1972; Hoefs, 1997; Baumgartner and Valley, 2001; Page *et al.*, 2013; Martin *et al.*, 2014; White and Klein, 2014; Rubatto and Angiboust, 2015).

Modelling of oxygen isotopic fractionation has been traditionally addressed as equilibrium calculation between individual mineral couples. A alternative approach follows what extensively adopted in the last decades for thermodynamic modelling (see reviews by Lanari and Duesterhoeft, 2018; Powell and Holland, 2008; Spear et al., 2017) and considers an evolving mineral assemblage. A pioneer model was proposed by Kohn (1993), limited to single and closed chemical systems, i.e. for which no infiltration of external fluids in isotopic disequilibrium was allowed. Such approach can evaluate how the oxygen isotopic composition changes with P and T, but it remains too simple for subduction zone settings, where significant fluid exchange occurs between different lithologies within the subducting slab. Baumgartner and Valley (2001) proposed a continuum mechanics model for stable isotope fluid-rock exchange, where infiltration profiles can be calculated, but no information is provided about the different components (minerals) of the rock, as it is considered as a continuum. The fluid/rock (F/R) ratio obtained with this strategy do not correspond to the physical fluid amount of fluid, but just represents a measurement of exchange progress.

We present a new approach that combines thermodynamics and oxygen isotope fractionation modelling applied to multi-rock systems. This modelling technique takes advantage of the increased capability of forward modelling of complex systems achieved in last two decades. A MATLAB©-based modelling program PTLOOP has been developed to calculate oxygen isotope fractionation between stable phases from the results of Gibbs energy minimization performed by Theriak-Domino (de Capitani and Brown, 1987; de Capitani and Petrakakis, 2010) along any fixed P-T trajectory. The oxygen isotope variation of each mineral within the evolving assemblage is tracked using an extensive and internally consistent database for oxygen isotope fractionation (Vho et al. in review). A graphical user interface (GUI) provides the representation of the results. The capabilities of this software solution will be discussed in details with an example that focuses on the characterization of (1) the effect of the dehydration reactions on the bulk $\delta^{18}O$ of a rock, (2) the effect of the influx into a subducting rock of an external fluid of distinct isotopic signature and (3) the final amount and isotopic signature of the fluid leaving the multi-rock system, e.g. infiltrating an upper unit or the mantle wedge. Petrological implications of relevant computational results are also discussed.

2 Modelling

2.1 Model geometry

On average, the subducting oceanic lithosphere is composed of a section of oceanic crust with its sedimentary cover (mostly < 1 km) above, and an ultramafic lithospheric mantle section beneath. The geometry of the model is illustrated in Fig. 1. The target column represents a simplified section of the upper part of such oceanic lithosphere. It is composed of a layer of basaltic composition (*Rock1*) overlaid by a layer of sediments (*Rock2*, see below for details). Two different rock columns are considered: a relatively "wet" system with altered basalts and terrigenous sediments, and a relatively "dry" system with fresh MORB and carbonates. The column has a fixed section of 1 m^2, while the thickness of each rock unit can be set by the user. The model is conservative with respect to the mass, while the volume of each rock type is changing according to fluid loss and density variation along the P-T path. The P-T structure of subduction zones depends on numerous variables, including the age of the incoming lithosphere and the amount of previously subducted lithosphere (e.g., Peacock, 1990). In this study, the calculation was performed following the subduction geotherm from Gerya *et al.*, (2002) (Fig. 2) over a pressure range of 1.3 – 2.6 GPa, corresponding to a depth of ~ 45 to ~ 85 km to encompass the conditions of interest for the investigated processes. The modelled temperatures range from a minimum of 350 °C to a maximum of 700 °C. The lower limit is due to the large uncertainties in the thermodynamic

https://doi.org/10.5194/se-2019-140
Preprint. Discussion started: 23 September 2019

databases for many common low-T metamorphic minerals that lead to not satisfactorily models for phase equilibria and mineral parageneses for low-grade metabasites (Frey et al., 1991). The upper limit is fixed before the melting region of metasediment – the present model strictly applies to subsolidus conditions.

During burial and heating the different slab lithologies undergo dehydration reactions. The produced fluid escapes from the source rock and migrate upward, likely interacting with the surrounding units of different chemical and isotopic composition. The effect of an external fluid input on the $\delta^{18}O$ value of growing minerals is strongly dependent on the isotopic composition of the infiltrating fluid ($\delta^{18}O_{fluid}$) and on the degree of fluid/rock interaction (fluid-rock ratio, expressed as mass ratio). To explore different scenarios, three models are discussed involving different associations of fresh or altered oceanic basalts with terrigenous or calcareous sediments (Fig. 1b): (1) the interaction between the oceanic crust derived fluid and the overlying sediment is negligible and the two rocks evolve independently (*No Interaction* case, *NI*), (2) part of the oceanic crust derived fluid (50% when not specified differently) equilibrates with the sediment, while the other part leaves the system (*Partial Interaction* case, *PI*) and (3) all the fluid released by the MORB equilibrates with the sediment before escaping the system (*High Interaction* case, *HI*).

The thickness and the degree of serpentinization of the lithospheric mantle subducting beneath the oceanic crust can be highly variable. The most important dehydration reactions in these rocks are related to antigorite breakdown, which can release up to 12 wt% of water, playing an important role for water flows in subduction zones. Deserpentinization is assumed to result in two main subsequent fluid peaks (Padrón-Navarta et al., 2013; Scambelluri et al., 2004) related to the reactions

antigorite + brucite → olivine + chlorite + water (~ 480 °C, 1.7 GPa; 1 to 2 wt% water released, up to ~ 50 kg/m^3) (1)

antigorite → olivine + orthopyroxene + chlorite + water (~ 660 °C, 2.5 GPa; ≥ 6.5 wt% water released, ≥ 170 kg/m^3) (2)

The effect on the $\delta^{18}O$ of oceanic crust and sediments of an external fluid influx, i.e. caused by dehydration of the underlying serpentinites, was investigated by defining an amount of fluid with a specific $\delta^{18}O$ value that infiltrates *Rock 1* at two steps of the model (480 °C and 660 °C) (Fig. 1c,2).

2.2 Model strategy

The strategy behind PTLOOP consists of forward modelling the evolution of the mineral assemblage and the oxygen isotope composition of a rock column composed by two lithologies (Fig. 1a) of assigned thickness and starting bulk chemical and oxygen isotope compositions along a defined Pressure (P) -Temperature (T) path using a stepwise procedure (Fig. 2). At each P-T step, (1) the equilibrium mineral assemblage, oxygen isotope composition of stable phases, mass (in kg) and isotopic signature ($\delta^{18}O$ ‰ vs. Standard Mean Ocean Water, SMOW) of the excess fluid for the metabasalts are calculated; (2) any fraction of excess fluid deriving from dehydration reactions in the metabasalts can be transferred to the metasediments or directly escapes the system; (3) the equilibrium mineral assemblage, $\delta^{18}O$ value of stable phases, amount and signature of the excess fluid for the metasedimens are evaluated by accounting the changes caused by the fluid input from the metabasalts; (4) the mass (in kg) and $\delta^{18}O$ signature of the total fluid leaving the system is calculated. Furthermore, at each step a chosen amount of external fluid with a given $\delta^{18}O$ can be input in the metabasalts and its contribution is accounted in the subsequent steps. This model is based on the assumption of thermodynamic equilibrium applied to a partially reactive system, whereby phases are assumed to reach chemical and isotopic equilibrium at all steps within the reactive part of the system, i.e. excluding the phases that are fractionated (Lanari and Engi, 2017). Such petrological models can account for element sequestration during prograde metamorphism. Mineral fractionation in relicts and fluid input/loss are two processes that are allowed to modify the reactive bulk composition. No mineral resorption is permitted. Any fluid liberated during dehydration (excess fluid) does not further interact and leaves the rock. This process is termed *Rayleigh volatilization* (Rumble, 1982; Valley, 1986). In natural rocks, it occurs often combined with the opposite end-member, the *batch volatilization*, where the produced fluid stays within the system as the mineral reaction proceeds, and remains in isotopic equilibrium with the rock until the reaction is complete. In most natural cases involving oxygen isotopes, the difference

https://doi.org/10.5194/se-2019-140
Preprint. Discussion started: 23 September 2019

between the results calculated using the two processes is negligible (Baumgartner and Valley, 2001). The released fluid is considered as pure H_2O; therefore any other solute-transport effect is ignored.

2.3 Governing equations

Equilibrium assemblage calculation for a given bulk rock composition at any P and T is performed with the software Theriak (de Capitani and Brown, 1987; de Capitani and Petrakakis, 2010) and is based on Gibbs energy minimization. A complete description of the Theriak algorithm is given by de Capitani and Brown (1987). The reacting bulk composition may evolve in the course of the metamorphic history of a rock because of mineral fractionation, fluid loss or input of external fluids. The effective bulk composition is recalculated by PTLOOP at each subsequent stage following the strategy of Lanari *et al.* (2017).

As for phase assemblage determination, equilibrium is a common assumption of stable isotope transport (Baumgartner and Rumble, 1988; Baumgartner and Valley, 2001; Bowman et al., 1994; Gerdes et al., 1995a, 1995b). Thus, a molar equilibrium constant (*K*) can be defined to describe the thermodynamic stable isotope equilibrium between two substances *i* and *j* (Sharp, 2017)

$$K = \frac{{}^{18}O_i/{}^{16}O_i}{{}^{18}O_j/{}^{16}O_j} \quad (3)$$

The fractionation factor (α) can be related to the equilibrium constant K as

$$\alpha = K^{1/n} \quad (4)$$

where *n* is the number of exchanged atoms, normally 1 for simplicity. In isotope geochemistry, the isotopic composition is commonly expressed in terms of δ values

$$\delta_i = \left(\frac{R_i}{R_{St}} - 1\right) \cdot 10^3 \ (‰) \quad (5)$$

where R_i and R_{st} are the isotope ratio measurements for the compound *i* and the defined isotope ratio of a standard sample respectively. For differences in δ values or for δ values of less than ~ 10 ‰, it is valid the approximation

$$1000 ln\alpha_{i-j} = \delta_i - \delta_j \quad (6)$$

that is used in most cases (Hoefs, 1997; Sharp, 2017). For oxygen isotope fractionation, the equation that can reproduce most of the available calibrations describing the stable isotope fractionation function between two phases is a second order polynomial of $10^3/T$. Hence the stable isotope fractionation between two phases *i* (with *k* end-members) and *j* (pure) as a function of *T* is described by Eq. (7):

$$\delta^{18}O_i - \delta^{18}O_j = \sum_1^k \left(\frac{A_{k,j} \cdot 10^6}{T^2} + \frac{B_{k,j} \cdot 10^3}{T} + C_{k,j}\right) \cdot X_{k,i} \cdot \frac{N_{k,i}}{N_i} \quad (7)$$

and the conservation of the bulk $\delta^{18}O$ in the system by Eq. (8):

$$\delta^{18}O_{sys} \cdot N_{sys} = \sum_{k=1}^{p} M_k \cdot N_k \cdot \delta^{18}O_k \quad (8)$$

where $\delta^{18}O_i$, $\delta^{18}O_j$ and $\delta^{18}O_{sys}$ are the isotopic compositions of phase *i*, phase *j* and the system (bulk $\delta^{18}O$) respectively, $A_{k,j}$, $B_{k,j}$ and $C_{k,j}$ the fractionation parameters for end-member *k* of mineral *i vs.* phase *j*, $X_{k,i}$ the fraction of end-member *k* in the phase *i*, $N_{k,i}$, N_i and N_{sys} the total number of moles of oxygen in end-member *k*, in mineral *i* and in the system respectively, *p* is the number of phases, M_k the number of moles of phase *k*, N_k the its number of oxygen and $\delta^{18}O_k$ its oxygen isotope composition. Given a stable mineral assemblage at any P-T condition, the oxygen isotope partitioning among the stable phases is calculated by solving the linear system described by the sets of *p*-1 Eq. of type (7) and the Eq. (8) (Kohn, 1993; Vho et al. in review). In closed systems, the first term in Eq. (8) is constant. Open system behaviour can either modify the $\delta^{18}O_{sys}$ or the number of moles of the

https://doi.org/10.5194/se-2019-140
Preprint. Discussion started: 23 September 2019

phases (N_{sys}). The parameters *A*, *B* and *C* between phases were taken from the internally consistent database for oxygen isotope fractionation DBOXYGEN version 2.0.3 by Vho et al., in review.

2.4 Starting assumptions

In order to represent the variability in the basaltic portion of the oceanic crust two different bulk compositions were used (Table 1): (1) a representative unaltered oceanic basalt (Gale et al., 2013) and (2) a hydrated basalt (Baxter and Caddick, 2013 after Staudigel *et al.*, 1996). Those compositions are in good agreement with other compilations reported in literature (e.g., Sun and McDonough, 1989; Albarède, 2005; Staudigel, 2014; White and Klein, 2014). Oceanic sediments were modelled with two distinct bulk compositions (Table 1): (1) terrigenous sediment (clay from Mariana trench, Hacker, 2008 after Plank and Langmuir, 1998) and (2) nanno ooze carbonate sediment (Plank, 2014). Nanno ooze are widespread carbonate sea-floor sediments (Plank, 2014) and they are close in composition to carbonate-rich sediments observed in HP terrains (e.g., Bebout et al., 2013; Kuhn et al., 2005). Thicknesses of 1000 m for the basaltic layer, of 175 m for the clay sediment and 75 m for the carbonatic sediment were chosen in order to maintain proportions between oceanic crust and sediments comparable with the values reported in various compilations (e.g., Hacker, 2008; Plank, 2014). This results in a total thickness of the rock column 2 to 3 times smaller than natural profiles to encompass the assumption of homogeneous temperature over the whole column within ~ 20 °C. To overcome the effects of possible temperature variations within the column, a discretization step size of ~ 20 °C along the P-T path was applied.

The bulk compositions were simplified to the Na_2O–CaO–K_2O–MgO–FeO–Al_2O_3–TiO_2–SiO_2–H_2O system. MnO was excluded because it overemphasizes the stability of garnet at low metamorphic conditions (T ≤ 350 °C). The conditions of the garnet-in reaction in Mn-absent systems (MORB, altered MORB) match the results obtained for garnet nucleation in natural rocks (e.g., Laurent et al., 2018). Thermodynamic modelling was performed using the internally consistent dataset of Holland and Powell (1998) and subsequent updates (tc55, distributed with Theriak-Domino 04.02.2017, see Supplementary material S1). The following activity models where used for the solid solutions: Holland and Powell (2003) for calcite-dolomite-magnesite; Holland and Powell (1998) for garnet, white mica and talc; Holland and Powell (1996) for omphacite; Holland et al. (1998) for chlorite; Diener et al. (2007) for amphibole. In the presented model garnet undergoes fractional crystallization both in *Rock 1* and *Rock 2* fractionating the reactive bulk for the following steps. The amount of initial H_2O in each rock was set at saturation and is reported in Table 1. No pore fluid expulsion, diagenetic and low-grade (T < 350 °C) devolatilization reactions are considered in this study (see above).

A starting bulk $\delta^{18}O$ for the MORB of 5.7 ‰ was chosen and represents the reference value for an unaltered MORB (e.g., Cartwright and Barnicoat, 1999; Eiler, 2001; Staudigel, 2014; White and Klein, 2014), while a starting bulk $\delta^{18}O$ of 9.0 ‰ is representative of basaltic material that underwent sea-floor alteration at T ≤ 400 °C (e.g., Alt et al., 1986; Cartwright and Barnicoat, 1999; Eiler, 2001; Gregory and Taylor Jr, 1981; Miller and Cartwright, 2000; Staudigel, 2014; White and Klein, 2014). The starting bulk of the terrigenous sediment of 15 ‰ represents the average for the $\delta^{18}O$ of clastic sediments reported by Eiler (2001). The chosen $\delta^{18}O$ starting bulk of the carbonate sediment is 25 ‰, which represents a conservative estimate of marine carbonate $\delta^{18}O$ (typically 25 – 35 ‰, Eiler, 2001). It is ~ 5 ‰ higher than the values for metasedimentary carbonates in the Italian Alps (e.g., Cook-Kollars et al., 2014) that are likely to have interacted with lower- $\delta^{18}O$ fluids during subduction.

In order to define the contribution of an external fluid originating in the lithospheric mantle by serpentine breakdown, a layer of 150 m of pure serpentine containing 12 wt% bulk H_2O was considered and the mass of water released at each reaction was calculated by mass balance, resulting in and input of 7800 kg of water at 480 °C and of 25350 kg at 660 °C to satisfy reactions (#7) and (#8) respectively. In order to fit the thicknesses chosen for the oceanic crust and the sedimentary layer (2 to 3 times thinner than an average lithospheric section), the 150 m of pure serpentine correspond to a conservative estimate of 3000 m of serpentinized peridotite with an average serpentine content of 5 % in volume. This is in agreement with the values used by Barnes

https://doi.org/10.5194/se-2019-140
Preprint. Discussion started: 23 September 2019

and Straub (2010) and John *et al.* (2011) based on the estimate by Sharp and Barnes (2004). Serpentine oxygen isotope compositions reported in literature are highly variable (Cartwright and Barnicoat, 1999, 2003; Früh-Green et al., 2001; Mével, 2003; Miller et al., 2001), typically ranging from 1 to 10 ‰. In mid-oceanic ridge environments, the distribution has a peak between 2 and 5 ‰ (Mével, 2003). A value of 2.5 ‰ was chosen from the lower-$\delta^{18}O$ side of this peak, as the effect of interaction with the overlying, higher- $\delta^{18}O$, rocks is expected to become smaller when the two isotopic compositions get closer to each other. This leads to a $\delta^{18}O$ value of the released fluid of ~ 4.5 ‰ (serpentine/water fractionation factors compiled in Vho et al., in review). Further details on the modelling input data are given in Supplementary material S2.

3 Results

3.1 Stable mineral assemblage

The evolving stable mineral assemblages and bulk water contents of each lithology, without external fluid input, were calculated for each rock composition along the prograde P-T-path. Results are provided as mode-box diagrams in Fig. 3. The H_2O field represents the volume fraction of excess water in each rock type. The fluid is progressively extracted becoming isolated from the reactive part of the system. Garnet is the only phase prevented from re-equilibrating in the model, thus fractionating from the reactive bulk composition. Below 450 °C and 1.80 GPa, for the MORB compositions, glaucophane, actinolite and lawsonite comprise ~ 80 vol. % of the paragenesis, with minor white mica, omphacite, chlorite and titanite. The fresh MORB is richer in SiO_2, FeO and MgO with respect to the altered MORB and chlorite is stable up to 480 °C. Altered MORB contains ~ 5 vol% of Ca-carbonate that remains stable over the entire P-T-path. In either compositions, from 480 °C and ~ 1.90 GPa, the volume of glaucophane, actinolite and lawsonite gradually decreases until complete consumption at 600 – 620 °C and ~ 2.30 GPa. Those represent the major hydrous phases contributing to the dehydration, while a secondary role is played by talc and zoisite at higher conditions ($T \geq 580$ °C, $P \geq 2.24$ GPa). Most of the water still retained in the rocks is stored in white mica, the abundance of which is primarily controlled by bulk K_2O content, higher in the altered MORB, and that remains stable beyond the model conditions. Garnet production starts at ~ 500 °C and ~ 2.00 GPa in the MORBs and it grows continuously until constituting ~ 20 vol% of the altered MORB, ~ 35 % of the fresh MORB.

In the carbonate sediment at 350 °C and 1.30 GPa calcium carbonate, quartz, phengite and omphacite compose ~ 80 vol% of the solids. Glaucophane and lawsonite are stable up to 460 °C and 560 °C respectively. Glaucophane is consumed in favour of jadeite and ankerite, and lawsonite breakdown produces garnet. The terrigenous sediment shows a paragenesis of white mica, glaucophane, lawsonite, quartz and omphacite, with minor titanite, at $T < 500$ °C. At 500 °C and 2.00 GPa, lawsonite is consumed and the amphibole proportion reduces from ~ 30 vol% to < 20 vol% producing garnet. The clinopyroxene composition changes from omphacite to jadeite. Also in the terrigenous sediment, garnet appears at ~ 500 °C and ~ 2.00 GPa and it reaches ~ 15 vol% of the terrigenous sediment. In the carbonate sediment, garnet is stable only at 540 – 580 °C and 2.12 – 2.24 GPa reaching ~5 vol% and is then preserved because of the assumption of fractionation from the bulk in the model. These models are in line the first-order mineralogical changes observed in subducted (and exhumed) crustal material. Thermodynamic calculations predict the coexistence of a calcic amphibole and a sodic amphibole in the MORBs and of jadeite and omphacite in the terrigenous sediment. From an oxygen isotope partitioning perspective, the interpretations of the modelled coexistence of a sodic and a calcic amphiboles either as two end-members of a solid solution or as coexisting minerals are equivalent. Therefore, this does not affect the oxygen partition model final results for the other phases and the bulk.

https://doi.org/10.5194/se-2019-140
Preprint. Discussion started: 23 September 2019

3.2 Production of water

At the initial conditions, all the lithologies are saturated in H_2O (Table 1). Up to 500 °C, lawsonite, actinolite and glaucophane are the main repositories of H_2O in the MORBs, followed by chlorite in the fresh MORB and minor phengite. A significant pulse of water is modelled at 500 – 520 °C and 2.00 – 2.60 GPa in the fresh and altered MORB (Fig. 3a,b). This pulse is caused by decreasing abundance of lawsonite and amphiboles and breakdown of chlorite to produce garnet and omphacite. This first dehydration stage releases ~ 25 % of the total water loss from the altered MORB (~ 4.0 vol% H_2O liberated) and ~ 45 % from the fresh MORB (~ 6.5 vol% H_2O liberated). The second significant pulse in MORBs occurs at 620 – 640 °C and 2.36 – 2.42 GPa, releasing ~ 40 % of the total water loss from the altered MORB and ~ 15 % from the fresh MORB. This pulse is caused by the final breakdown of lawsonite and in the altered MORB of amphibole (Fig. 3b). In the fresh MORB, glaucophane and actinolite breakdown takes place at 600 °C and 2.03 GPa, causing an intermediate fluid pulse of minor magnitude (Fig. 3a).
The carbonate sediment is the composition that dehydrates the least: the two main pulses of fluid production are at 480 °C and 1.92 GPa (~ 0.4 vol% H_2O liberated) and from 540 °C and 2.12 GPa to 560 °C and 2.18 GPa (~ 1.7 vol% H_2O liberated), caused by breakdown of glaucophane and lawsonite respectively (Fig. 3c). The water produced from these two dehydration stages represents < 0.02 wt% of the total water released by the system composed by fresh MORB and carbonate sediment. In the terrigenous sediment the main fluid pulse occurs at 520 °C and 2.06 GPa (~ 3.0 vol% of H_2O liberated), caused by the breakdown of lawsonite and a decrease of glaucophane at the expense of garnet and clinopyroxene growth (Fig. 3d). The water produced from this dehydration stage represents ~ 0.07 wt% of the total water released by the system composed by altered MORB and terrigenous sediment.

3.3 Oxygen isotope compositions

The largest initial bulk $\delta^{18}O$ difference occurs between fresh MORB and carbonate sediment (14.3 ‰, the relatively dry system), while the smallest initial bulk $\delta^{18}O$ difference is observed between altered MORB and terrigenous sediment (6.0 ‰, the relatively wet system). In the following, the results are presented in details for a selection of two end-member scenarios (Fig. 4) (1) carbonate sediment associated to fresh MORB and (2) terrigenous sediment associated to altered MORB when not specified differently. Other scenarios (i.e. fresh MORB associated with the terrigenous sediment and altered MORB associated with the carbonate sediment) give intermediate results in terms of oxygen isotope composition variations as consequence of fluid/rock interaction. Further details and the results for the intermediate scenarios are given in Supplementary Material S3.

3.3.1 Bulk oxygen isotope compositions

For rocks that undergo only dehydration reactions the staring bulk $\delta^{18}O$ evolves as consequence of garnet and fluid fractionation (black solid lines in Fig. 4). The bulk $\delta^{18}O$ shift related to water fractionation is within 0.2 ‰, while the shift due to garnet fractionation is within 0.5 ‰ (Fig. 4c,d). Since water has typically heavier $\delta^{18}O$ signature with respect to the bulk and the garnet a lighter one, the two effects produce opposite trends. The combination of both effects results in a shift of the bulk $\delta^{18}O$ in the considered lithologies restricted to < 0.3 ‰. This in turn leads to negligible (< 0.2 ‰) variations in the $\delta^{18}O$ values of the stable phases.
In the metasediments, the progressive interaction with the fluid from the mafic rocks causes a decrease in the bulk $\delta^{18}O$ (Fig. 4g,h) that is controlled by the amount and signature of the incoming fluid. A significant decrease starts at 480 °C where the amount of water released by mafic rocks increases of about one order of magnitude from < 0.05 vol% to ~ 0.3 vol% due to partial consumption of amphiboles and lawsonite. The maximum shift in bulk $\delta^{18}O$ was calculated for the carbonate interacting with the fresh MORB at ~ 12.9 ‰ for the *HI* case, while it is ~ 8.7 ‰ for the *PI* case. The shift of the bulk $\delta^{18}O$ of the terrigenous sediment interacting with the altered MORB is ~ 1.5 ‰ for the *HI* case and ~ 2.7 ‰ for the *PI* case.

https://doi.org/10.5194/se-2019-140
Preprint. Discussion started: 23 September 2019

3.3.2 Oxygen isotope composition of mineral phases

Since at infinite temperature the fractionation between any two phases approaches 0 ‰, a general trend of reduction of oxygen isotope fractionation between the stable phases with increasing metamorphic grade is observed in all lithologies and is a result of the temperature increase (coloured lines in Fig. 4a,b,e,f). As a consequence, mineral phases typically heavier than the bulk (i.e. quartz and carbonates) become isotopically lighter with increasing metamorphic conditions, and the mineral phases typically lighter than the bulk (i.e. rutile, garnet and titanite) become isotopically heavier. Such variations are limited (i.e. within 1.0 ‰) for most of the phases, with the exception of quartz, calcite and rutile that may vary up to 3.0 ‰ in response to temperature variation only in the considered range.

In the case of ingress of the low $\delta^{18}O$ fluid from the MORB in the sedimentary rocks (*PI* and *HI* cases), the mineral $\delta^{18}O$ values decrease progressively with respect to the *NI* case following the trend of the bulk $\delta^{18}O$ (Fig. 4g,h). For instance, in case of *NI* the $\delta^{18}O$ of quartz in the terrigenous sediment decreases from 19.4 ‰ to 17.3 ‰ (- 2.1 ‰) and quartz in the carbonate sediment from 28.0 ‰ to 26.5 ‰ (-1.5 ‰) because of increasing temperature. In the *PI* and *HI* cases, the $\delta^{18}O$ shift of quartz is respectively -3.8 ‰ and -5.0 ‰ in the terrigenous sediment, -10.0 ‰ and -13.9 ‰ in the carbonate sediment. Hence, the final quartz $\delta^{18}O$ values (at 700 °C, 2.60 GPa) for the *HI* case in the terrigenous and in the carbonated sediment are respectively 3.0 ‰ and 13.0 ‰ isotopically lower than the expected in case of *NI* (Fig. 4e-h). The maximum shift of $\delta^{18}O$ (i.e. between *NI* and *HI* cases) for the other stable phases is within those values. In the terrigenous sediment, the $\delta^{18}O$ values of phengite, galucophane, jadeite, rutile and garnet decrease by 3.0 ‰ and of omphacite by 2.4 ‰ from the *NI* to the *HI* case. Lawsonite and titanite are not stable after the first significant mafic fluid input (500 °C, 2.00 GPa), and their $\delta^{18}O$ values decrease of 1.1 ‰ and 0.3 ‰ respectively from the *NI* to the *HI* case. In the carbonate sediment, the $\delta^{18}O$ values of dolomite, jadeite, phengite, rutile and aragonite decrease of maximum 13.1 ‰, of lawsonite and ankerite of maximum 10.3 ‰ and 9.5 ‰ respectively. Garnet crystallizes only between 540 °C and 580 °C and its $\delta^{18}O$ value in the *HI* case is 5.9 ‰ lower than the one in the *NI* case.

3.3.3 Oxygen isotope composition of the fractionated fluids

The $\delta^{18}O$ of the fractionated water from each rock type at each step is in isotopic equilibrium with the stable mineral assemblage at the given conditions. In the temperature range where the most fluid is released (i.e. T > 480 °C) the $\delta^{18}O$ of the mafic fluid is 7.0 ± 0.5 ‰ for the fresh MORB and 10.0 ± 0.5 ‰ for the altered MORB. At T > 480 °C, the water released in the *NI* case by the carbonate sediment has a $\delta^{18}O$ = 24.2 – 25.6 ‰ and from the terrigenous sediment of 15.4 – 16.4 ‰ (Fig. 5). The $\delta^{18}O$ of the fluid leaving the system, e.g., infiltrating an upper layer or the mantle wedge, results from the mixing of the water released from the MORB and overlying metasediment and the balance between the amount of fluid released by each rock type and its $\delta^{18}O$ value (blue lines in Fig. 5a,b).

In the *NI* case, the $\delta^{18}O$ of water leaving the system is up to 1 ‰ higher than the composition of the fluid released by the MORB because of the minor input from the metasediment at around 500–550°C. The only exceptions are for the interaction between altered MORB and the terrigenous sediment at T of ~ 450 °C and ~ 700 °C. At these conditions, the $\delta^{18}O$ values of the final fluid are up to 5 ‰ higher than the mafic fluid (thick dark blue line in Fig. 5b). This increase is caused by a proportion in favour of the sedimentary fluids at those conditions; however, the amount of high-$\delta^{18}O$ fluid represents < 0.1 wt% of the rock column and ~ 1 wt% of the total released fluid (grey field in Fig. 5b).

In the case of interaction between the sediment and the mafic fluid, part or all the mafic fluid reacts with the sediment before leaving the system and the final $\delta^{18}O$ signature of the fluid is controlled by the mafic fluid/rock ratio in the sediments and their buffering capacity. In the *HI* case, the $\delta^{18}O$ of the released fluid has a dominant sedimentary signature before the first fluid pulse from the MORBs (T < 500 – 520 °C) (14.5 – 15.5 ‰ for the terrigenous sediment and 23.0 – 24.0 ‰ for the carbonate sediment, light blue lines in Fig. 5). The first mafic fluid pulse (500 – 520 °C, see above) causes a drop in the bulk $\delta^{18}O$ values of released fluids of 0.7 ‰ for the altered MORB/terrigenous sediment association and of 6.3 ‰ for the fresh MORB/carbonate sediment

https://doi.org/10.5194/se-2019-140
Preprint. Discussion started: 23 September 2019

association. The second mafic fluid pulse (620 – 640 °C, see above) causes a second decrease of the $\delta^{18}O$ values of the released fluid equal to 1.0 ‰ for both the lithological associations.

3.3.4 Input of ultramafic fluid

Ultramafic rocks tend to undergo episodic dehydration (see above). In the following, the effects caused by the input of an ultramafic fluid at the base of the rock column in case of *HI* are described (Fig. 6). In the *PI* and *NI* cases, the effect of the ultramafic fluid on the MORB remains the same, while the variations in the sedimentary rocks will decrease to zero (Supplementary Material S3). The input of the amount of water corresponding to the dehydration of 150 m of pure serpentine at 480 °C (2.0 wt% H_2O) and 660 °C (6.5 wt% H_2O) having a $\delta^{18}O$ = 4.5 ‰, (see above) produces a decrease of < 0.2 ‰ in the final bulk $\delta^{18}O$ of the MORBs, up to ~ 1.0 ‰ in the carbonate sediment (Fig. 6a) and of < 0.5 ‰ in the terrigenous sediment (Fig. 6b) with respect to the *HI* case without ultramafic fluid. The largest decrease occurs at 660 °C, where the second pulse of ultramafic fluid enters the system, resulting in ca. -0.1 ‰, -0.3 ‰ and -1.0 ‰ for the MORBs, the terrigenous sediment and the carbonate sediment respectively (Fig. 6). Even by increasing the thickness of the serpentinite by a factor of two, the variations in bulk $\delta^{18}O$ values are < 1.0 ‰ for any rock type with the exception of the carbonate sediment, for which the bulk $\delta^{18}O$ decreases of 2.0 ‰ with respect to the ultramafic fluid-absent *HI* case (Supplementary Material S3).

4 Discussion

4.1 Effect of stable assemblage evolution and phase fractionation on the bulk $\delta^{18}O$

The changes in mineral assemblage, modes and compositions along a prograde *P-T* path control (1) the oxygen isotope partitioning between the stable phases and (2) the amount and $\delta^{18}O$ of the water released by the system. At the same time, oxygen isotope fractionation between the stable phases is controlled by temperature. Thus, the effects of evolving paragenesis and increasing temperature are systematically overlapping in nature. In the case of a closed system, the bulk concentrations of ^{18}O and ^{16}O remain constant and a change in one phase is compensated exactly by adjustments in other phases (Baumgartner and Valley, 2001; Kohn, 1993). In this situation, major changes in mineral assemblage do not play a significant role in shifting the $\delta^{18}O$ of stable phases: this is demonstrated by the limited (< 0.5 ‰) shift in $\delta^{18}O$ value of quartz, garnet, phengite, omphacite and rutile in the MORB after (1) breakdown of amphibole and lawsonite and (2) crystallization of talc and kyanite over a narrow T range between 500 and 580 °C (Fig. 4a,b). The limited effect of changing assemblages on the variation in oxygen isotope composition can be evaluated with an extreme example. A granite composed of quartz + K-feldspar + plagioclase + biotite + accessory ilmenite and zircon at 700 °C and 0.3 GPa is subducted to 700 °C and 2.5 GPa. If lack of hydration prevents the rock from re-equilibration, the granite can preserve a metastable mineral assemblage during subduction. Assuming a pervasive hydration at 700 °C and 2.5 GPa, a re-equilibration into a full eclogite facies assemblage of quartz + white mica + garnet + clinopyroxene + accessory rutile and zircon occurs. The temperature was kept constant in order to remove any T-related effect and the fluid was assumed to be in equilibrium with the mineral assemblage. Quartz $\delta^{18}O$ variation between the two parageneses, as well the difference between ilmenite and rutile $\delta^{18}O$, are within 1 ‰.

In a closed system evolving at equilibrium, the initial bulk composition and bulk $\delta^{18}O$ do not change along the P-T evolution. However, in metamorphic rocks, compositional zoning and metamorphic overgrowths are often preserved in refractory minerals (Lanari and Engi, 2017) indicating that parts of the minerals became isolated from the reactive volume of the rock. This scenario is referred as partially re-equilibrated open systems, because the chemical and the isotopic compositions vary as a consequence of fractionation of solid and fluid phases (i.e. garnet fractionation and excess fluid removal) even in absence of external fluid input. Phase fractionation is expected to affect the bulk $\delta^{18}O$ as function of both the amount of fractionated or expelled phases and their isotopic composition. Fractionation of a phase lighter than the bulk in $\delta^{18}O$ leads to an increase in bulk $\delta^{18}O$, while fractionation of

https://doi.org/10.5194/se-2019-140
Preprint. Discussion started: 23 September 2019

an isotopic heavier phase leads to a decrease in bulk $\delta^{18}O$. The most common example of fractionating metamorphic mineral is garnet, which systematically records compositional zonation at low- to medium-grade (Evans, 2004; Giuntoli et al., 2018; Konrad-Schmolke et al., 2008; Spear, 1988; Tracy, 1982). Therefore, garnet fractionation was incorporated in the model in order to better approximate the behaviour of natural systems. Note that this effect is reduced at higher grade where intra-crystalline diffusion becomes efficient to partially re-equilibrate garnet (Caddick et al., 2010; Lanari and Duesterhoeft, 2018). As already documented by Konrad-Schmolke et al. (2008), garnet fractionation controls the extend of the garnet stability field. Garnet crystallization is not systematically expected to occur near the peak conditions, if the matrix was strongly depleted due to garnet fractionation and the volume of garnet remains constant (i.e. for the altered MORB composition, Fig. 3b). While garnet fractionation is recognized to significantly affect isopleth thermobarometry and volume fractions (Lanari and Engi, 2017), its effect on oxygen isotope bulk composition and partitioning is negligible (< 0.5 ‰) in all the studied lithologies. In the model, the garnet fraction varies from ~ 5 vol% in the carbonate sediment to ~ 35 vol% in the fresh MORB (Fig. 3) and its $\delta^{18}O$ is 0.8 to 1.7 ‰ lower than the bulk (Fig. 4a,b,e,f). Beside garnet fractionation, dehydration due to hydrous mineral breakdown and expulsion of excess water may contribute to changing the starting chemical and isotopic bulk compositions. Baumgartner and Valley (2001) postulated that the liberation of metamorphic fluids might have a profound effect on the stable isotope composition of the residual rock. In the present study, the maximum fluid loss is from the MORBs that release ~ 15 vol% (~ 5 wt%) of H_2O with $\delta^{18}O$ values 0.9 to 1.5 ‰ higher than the bulk rock (Fig. 4a,b) at $T \geq 500$ °C. This significant fluid flux produces a decrease in the bulk $\delta^{18}O$ of less than 0.2 ‰ (Fig. 4c,d). Even if more extensive dehydration occurs, the effect on the value of $\delta^{18}O$ will be typically lower than 1 ‰. No significant differences in the effect of stable assemblage evolution and phase fractionation are observed between the four lithologies. Therefore, the bulk $\delta^{18}O$ of a rock that experienced a succession of dehydration reactions without rehydration by external fluids is likely to be representative of its protolith composition. In this regard, integrated thermodynamics and oxygen isotope modelling represents a key tool for quantifying the potential effects of different processes and for assessing closed or open system behaviours.

4.2 Mineral $\delta^{18}O$ zoning as indicator of open system behaviour

In the last decades, the significant advances of oxygen stable isotope analyses by SIMS (secondary ion mass spectrometer) allowed zoned metamorphic minerals to be analysed in situ with a precision down to 0.2 – 0.3 ‰ (2σ) (e.g., Martin et al., 2014; Page et al., 2010). The magnitude of the intra-crystalline $\delta^{18}O$ variation in key metamorphic minerals has been widely used to target whether a metasomatic stage is related to an internal fluid deriving from the breakdown of hydrous phases or if it reflects equilibration with an external fluid of different isotopic composition (e.g., Putlitz *et al.*, 2000; Errico *et al.*, 2013; Page *et al.*, 2013; Russell *et al.*, 2013; Martin *et al.*, 2014; Rubatto and Angiboust, 2015; Engi *et al.*, 2018). Understanding the scale of fluid migration at depth and the magnitude of the interaction between fluids and minerals is of special interest and can be enhanced by modelling of such fluid flow and isotopic exchange (Baumgartner and Valley, 2001). The definition of different *interaction cases* (*NI*, *PI*, *HI*) is useful to represent various degrees of isotopic exchange between the fluid and the rock. If the flow is channelized, all the *interaction cases* can possibly occur in close proximity and the modelled scenarios can be linked to the evolution of different domains around the vein (Fig. 7). The flow of a pervasive fluid leads to homogenization of the chemical potential of all components, including stable isotopes (Baumgartner and Valley, 2001), and it is represented by the *HI* case, as long as integrated fluid/rock ratios are high. In contrast, the flow of a channelled fluid results in local chemical heterogeneities, allowing some portions of the rock and of the fluid to remain unaffected (*NI* case) and some other to be only partially affected (*PI* case).

The first step for a meaningful interpretation of an observed intra-grain variation in $\delta^{18}O$ value is the quantification of the possible effects of changes in T and mineral assemblage. Such effects are characteristic of each phase (Fig. 4a,b,e,f). Quartz, calcite and rutile are the most sensitive minerals to such changes. Their composition is expected to vary up to 1 ‰ per 100 °C and they are stable over a wide range of temperature. For such phases, care is required in interpreting significant intra-grain $\delta^{18}O$ variations (i.e. up to 3.0 ‰) since it does not necessarily reflect interaction with an external fluid having a different isotopic signature.

https://doi.org/10.5194/se-2019-140
Preprint. Discussion started: 23 September 2019

However, the variation of garnet $\delta^{18}O$ over 150 °C is typically within 0.5 ‰ when no phase fractionation is involved and still less than 1.0 ‰ when considering the effect of previous garnet and/or excess fluid fractionation (Fig. 4a,b,e,f). Thus, any larger variation has to be linked to a significant change in bulk $\delta^{18}O$. Similar behaviour is observed for other key metamorphic minerals such as white mica, amphibole and clinopyroxene. These minerals have been widely used in metamorphic petrology as thermometers and geobarometers (Dubacq et al., 2010; Ferry and Spear, 1978; Parra et al., 2002) and are expected to be robust targets to link the fluid evolution along the P–T path, especially when mineral relics are preserved. Due to its large capacity to preserve growth chemistry, garnet has been a primary target for microscale measurement of oxygen isotope. Protocols and reference materials for SIMS measurements for a range of garnet compositions are well established (e.g., Martin et al., 2014; Page et al., 2010; Vielzeuf et al., 2005) and its retentivity to high T resetting by diffusion has been investigated (Higashino et al., 2018; Vielzeuf et al., 2005a). Studies that used in-situ measurement of micas are limited (Bulle et al., 2019; Siron et al., 2017) and thus the potential of mica to trace fluid-rock interaction is still underexplored. The matrix complexity of pyroxenes and amphiboles remains a challenge for SIMS measurements.

4.3 Interaction with fluids from an ultramafic source

The effect of pervasive fluid flow deriving from serpentine breakdown ($\delta^{18}O$ = 4.5 ‰) on the bulk $\delta^{18}O$ of the fresh and altered MORBs calculated for different thicknesses of pure serpentine (150 m, 300 m, 600 m, see above) is negligible (< 0.5 ‰, Fig. 6, Supplementary Material S3). This is mainly due to (1) the minor difference in $\delta^{18}O$ between the ultramafic fluid and the MORB (1.2 ‰ for the fresh MORB and 4.5 ‰ for the altered MORB) and (2) the very low integrated F/R ratio (0.01, 0.02 and 0.04 for the 3 cases). The latter seems to play a bigger role, since the limited change in $\delta^{18}O$ is similar for both MORBs even if the initial difference in $\delta^{18}O$ between input fluids and receiving rock is larger for the altered MORB. With the same total volume of fluid and rock, a channelized fluid flow would imply larger volumes of fluid interacting with smaller volumes of rock (higher fluid/rock ratios) and would thus be expected to drive larger variations in isotopic composition. For instance, by increasing of a factor 10 the F/R ratio (from 0.01 to 0.1) the fresh and altered MORB bulk $\delta^{18}O$ decreases of 0.6 ‰ and 1.1 ‰ respectively.

In contrast to the MORB layers, the overlying sediments have (1) larger compositional differences with the ultramafic fluid and (2) a smaller mass. The consequence is that the effect of the ultramafic fluid input on the sediment bulk $\delta^{18}O$ compositions can be up to 10 times larger than in the MORBs, even when the ultramafic fluid completely equilibrates with the MORBs before interacting with the sediments. By applying a F/R ratio of 0.1, the final bulk $\delta^{18}O$ of the carbonate sediment decreases of 4.6 ‰ and of the terrigenous sediment of 2.6 ‰. These values are significant and demonstrate how sediments can be a good target to detect fluids from an ultramafic source migrating upward through the subducting slab or along the subduction interface, even though the two lithologies may not be in direct contact in the field.

It is important to note that the relatively “dry” system composed by fresh MORB and carbonate sediment is more sensitive to external fluid infiltration and thus affected by the highest changes in $\delta^{18}O$, according with observation in natural systems (e.g., Page et al., 2019).

4.4 Effect of the subduction geotherm

As discussed in detail by previous studies (Baxter and Caddick, 2013; Hacker, 2008; Hernández-Uribe and Palin, 2019; Syracuse et al., 2010), the subduction geotherm has an important effect on hydrous phase stability and P-T conditions of fluid release into the mantle wedge. Along the average D80 geotherm by Syracuse et al. (2010) (Fig. 2), the top of the slab crust releases ~ 95% of the water at ~ 80 km, during the transition from partial to full coupling. Along the cold geotherm by Penniston-Dorland et al. (2015), the first significant fluid pulse (20 – 40 % of water released) occurs as consequence of breakdown of glaucophane and actinolite at greater depths than predicted by our model (~ 500 °C and 2.7 – 2.8 GPa, 90 – 100 km depth) and the remaining water is released at depth > 100 km. Both those models imply a relatively dry mantle forearc region, contradicting what described by

https://doi.org/10.5194/se-2019-140
Preprint. Discussion started: 23 September 2019

Bostock et al. (2002). By contrast, along the warm geotherm by Penniston-Dorland et al. (2015), the breakdown of chlorite, epidote and actinolite releases 40 – 50 % of the water at 460 – 470 °C and ~ 0.6 GPa (~ 20 km depth); after this stage, ~ 95 % of the water is released at depth < 70 km. This implies that little to no water is available at subarc depths. The average geotherm by Penniston-Dorland et al. (2015) is hotter than the one by Gerya et al. (2002) used in our model for T < 650 °C and P < 2.5 GPa (Fig. 2). Along this P-T gradient chlorite is the main water carrier at low depths and the first two main dehydration pulses occur at depths of 30 – 40 km (significant decrease of chlorite, 20 – 25 % of water released) and of ~ 50 km (complete breakdown of chlorite, 20 – 25 % of water released). Along this geotherm, the most water is released at shallower depths than in our model. Differences can be investigated in detail by modelling each case with PTLOOP. Nevertheless, the effects of fluid-rock interaction on the bulk and mineral $\delta^{18}O$ compositions follow the general trends described above. Different parageneses are expected to form during hydration, but the shift in bulk $\delta^{18}O$ remains constrained by the F/R ratio and the isotopic composition of the incoming fluid.

4.5 Implication for mantle-wedge hydration

Infiltration of the slab-derived fluid into the mantle wedge is important for subduction zone settings because mantle minerals are strongly depleted in volatiles. At equilibrium, a free aqueous fluid is not stable in the mantle wedge at T < 650°C until a fully hydrated mineral assemblage has formed (i.e. serpentine, chlorite, talc, and amphibole) (Manning, 2004). As shown above, the P-T conditions of H_2O release from the subducting slab, as well as the volume and the $\delta^{18}O$ of the liberated H_2O can vary according to the geometry of the subduction zone and the composition of the subducting lithosphere (e.g., Hacker, 2008; Hernández-Uribe and Palin, 2019; Poli and Schmidt, 2002). The program PTLOOP allows the P-T conditions, amount and oxygen isotope composition of the released fluid to be calculated for the system of interest. The presented model uses an intermediate P-T gradient that stabilizes lawsonite and results in a first significant fluid pulse at 65 – 70 km depth and a second pulse at ~ 80 km depth. Below that depth, phengite is the main carrier of H_2O. This implies that the majority of fluid is released in the forearc region, in agreement with previous studies investigating the dehydration of MORB and sedimentary components of the slab (e.g., Baxter and Caddick, 2013; Kerrick and Connolly, 2001; Schmidt and Poli, 1994).

The influence of the slab-derived fluid on (1) the degree of hydration and (2) the $\delta^{18}O$ modification of the overlying mantle rocks was estimated on the basis of the results presented above. A slab composed by altered MORB and terrigenous sediments (left column in Fig. 1a, assuming the real thickness of the slab to be 3 times the modelled one) subducting at 1 cm/y was considered (Fig. 8a). This subduction rate represents a conservative estimate, considering an average of 4 – 5 cm/y (Stern, 2002). Mechanical decoupling between the slab and the wedge, and steady state cold mantle wedge are assumed (e.g., Abers et al., 2006; Hirauchi and Katayama, 2013; Wada et al., 2008). The fluid released by the slab at 500 – 520 °C with a characteristic $\delta^{18}O$ = 15.0 ‰ (Fig. 5a) was let infiltrate in an initially dry peridotite (composition KLB-1 from Walter, 1998, simplified to the FMAS system, Table S4 in Supplementary Material S2) with T = 570 °C and an initial $\delta^{18}O$ = 5.5 ‰ (Eiler et al., 1997; Mattey et al., 1994). This simplified model ignores the dynamics of fluid infiltration and assumes pervasive flow. The released fluid first interacts with a small volume at the slab-mantle interface (V1 1000 x 1000 x 1 m, Fig. 8b) and once it has equilibrated and saturated V1, it infiltrates volume V2 (3000 x 2000 x 1 m, Fig. 8b). Both the volumes were scaled to 1:3 for the calculation in order to maintain the volume proportion with the modelled slab. The slab-derived fluid, which is in continuous supply during subduction of new material, infiltrates V1 and causes a progressively change in mineralogy from olivine + orthopyroxene + garnet to serpentine + chlorite + minor olivine until the rock reaches saturation after 0.35 Myr of subduction. At this stage, V1 has a bulk $\delta^{18}O$ of ~ 8 ‰ that is significantly higher with respect to the initial value (Fig. 8c). With ongoing subduction, the continuing release of water from new slab material under a static mantle drives the $\delta^{18}O$ of the volume of mantle wedge toward higher values. The water that will infiltrate V2 has a $\delta^{18}O$ that depends on (1) the $\delta^{18}O$ of the slab-derived water and (2) the buffering capacity of V1. The same changes in mineral assemblage described for V1 occur also in V2, while the bulk $\delta^{18}O$ of V2 increases more moderately than the one of V1 and reaches a $\delta^{18}O$ of ~ 6 ‰ after 0.75 Myr of subduction.

https://doi.org/10.5194/se-2019-140
Preprint. Discussion started: 23 September 2019

In the proposed model, most of the fluid is released by the slab at forearc depths. However, in most subduction zones no melting appears to occur in the forearc region and the serpentinite acts as the effective H_2O-absorber (Iwamori, 1998), recording the possible variation in $\delta^{18}O$ induced by the slab-derived fluid. Progressive oceanward migration of the slab ("slab rollback") has been considered as an important mechanism acting in most active subduction zones (e.g., Heuret and Lallemand, 2005; Nakakuki and Mura, 2013). The rollback of the slab results in a lateral extension of the serpentinized wedge. As consequence, the melt ascending below the arc can interact with serpentinized, high $\delta^{18}O$ mantle portions that were originally part of the forearc mantle and modify its original isotopic composition. High $\delta^{18}O$ arc lavas have been described (e.g., Dorendorf et al., 2000; Eiler et al., 1998), but the mechanism of crustal contamination is still debated. Our results support the model proposed by Auer et al. (2009) that relates such high $\delta^{18}O$ lavas to the interaction between primitive basaltic melts with the uppermost mantle that was once hydrated and enriched as part of the forearc mantle prior to trench migration.

4.6 Model applications and future directions

The presented approach has a broad range of applications for modelling fluid/rock interaction in different tectonic settings. We have presented here an example of subducted crust but the same principles apply also for regional metamorphism or hydrothermal systems. The model also provides new ways to quantify the degree of interaction of an external fluid within the same rock unit. We have shown that the observed effect on the $\delta^{18}O$ of a rock of channelized *vs* extensive hydration is strictly coupled with the composition of the fluid source. Nevertheless, important insights can be given by linking observations of ideal cases with modelling even if the composition of the infiltrating fluid is not known a priori. For instance, the oxygen isotope composition of a fluid source can be retrieved when a variation in $\delta^{18}O$ is observed within the same rock type from the more hydrated to the less hydrated portions, even in absence of a clear presence of a vein or vein system. Alternatively, the degree of equilibration of the host rock around a vein can be calculated when the isotopic composition of the fluid is known. Therefore, the combination of mineral-scale in-situ oxygen isotope analyses with major and trace element mapping will provide much more detailed information on quantitative element mobility during fluid-rock interaction.

Fluids play a central role as catalyst for chemical reactions in rocks. Generally re-equilibration reactions occur only in presence of fluids that either derive from breakdown of hydrous phases or from external sources (e.g., Airaghi et al., 2017). The program PTLOOP calculates at which P-T conditions dehydration reactions occur and, consequently, metamorphic reactions and free fluid are expected. If in a rock mineral growth occurs at P-T conditions where no internal fluid is buffered, the role of an external fluid should be considered and its amount and isotopic composition can be retrieved using the approach outlined in this paper.

5 Conclusions

We developed a user friendly tool that combines equilibrium thermodynamic with oxygen isotope fractionation modelling for investigating the interaction between fluids and minerals in rocks during their metamorphic evolution. The program simulates along any given P-T path the stable mineral assemblages, bulk $\delta^{18}O$ and $\delta^{18}O$ of stable phases and the amount and oxygen isotope composition of the fluid released.

The capabilities of the program PTLOOP are illustrated by an application to subduction zones, but the presented modelling strategy can be applied to various metamorphic and tectonic settings. In this study, the chosen system represents a section of subducting oceanic crust composed by a lower layer of either fresh or altered MORB and an upper layer of sediments of carbonatic or pelitic composition. The calculation follows a step-wise procedure along the chosen P-T path. During the prograde evolution, any mineral and excess fluid can be fractionated from the reactive bulk composition.

Variations in $\delta^{18}O$ of stable phases due to mineral fractionation and/or excess fluid loss is typically negligible (i.e. < 0.5 ‰), while the effect of temperature variation over a range of ~150 °C on the mineral $\delta^{18}O$ is phase dependent and may be significant (> 1.0 ‰). Interaction with an external fluid of different oxygen isotope composition leads to shifts in bulk and mineral $\delta^{18}O$ values that

https://doi.org/10.5194/se-2019-140
Preprint. Discussion started: 23 September 2019

are marked when the major fluid pulses from the source rock occur, according to the degree of fluid/rock interaction and $\delta^{18}O$ difference between the rock and the fluid. Extreme large variations in bulk $\delta^{18}O$ of ~ 12 ‰ are calculated for the carbonate sediment equilibrating with a fresh MORB derived fluid, while small variations of ~3 ‰ are calculated for the terrigenous sediment equilibrating with an altered MORB derived fluid. When 50 % or more of the fluid deriving from dehydration of the basaltic crust equilibrates with any of the overlying sediments, the final $\delta^{18}O$ of the fluid released by the system has a dominant sedimentary signature, with values between 12 and 18 ‰. Such fluid with $\delta^{18}O$ values of 6.5 to 12.5 ‰ higher than the mantle value (5.5 ‰) have a great potential to modify the oxygen isotope composition of the mantle wedge at the slab-mantle interface. Extensive serpentinization and $\delta^{18}O$ increase of ~ 2.5 ‰ are modelled at the interface already after 0.35 Myr of ongoing subduction.

PTLOOP provides a powerful way to evaluate the effect of closed system *vs* open system behaviour with respect to oxygen isotopes during the evolution of the rocks. Different degrees of interaction between the external fluids and the sink lithology can be simulated and the effects of internally *vs* externally buffered fluids on the mineral paragenesis and on the mineral isotopic composition investigated.

Measured oxygen isotope compositions in minerals, intra-grain or bulk $\delta^{18}O$ variations at different scales, can be compared with the results of the model for specific scenarios. If the measured isotopic compositions are not consistent with the behaviour of a closed system, the presented model can be used to determine feasible external fluid sources, to estimate the degree of fluid-rock interaction and the metamorphic conditions at which this happened. Our model thus opens new avenues for mapping fluid pathways related to external fluid infiltration during the metamorphic evolution of the crust, with important consequences for element recycling in subduction zones and investigation of fluid-induced earthquakes.

Code availability

A compiled version of the program PTLOOP is available for download for the purpose of review at the temporary link https://www.dropbox.com/sh/h2objjchbd6plwv/AABzPSSPfKmG1KBxc-qiDPf2a?dl=0.

Author contributions

Alice Vho developed the model and performed the calculations. Pierre Lanari supervised the software development and contributed to the code implementation. Daniela Rubatto and Jörg Hermann contributed to formulate and design the model and to the interpretation of the results. Alice Vho prepared the manuscript with contributions from all co-authors. Daniela Rubatto conceived the project and secured funding.

Competing interest

The authors declare that they have no conflict of interest.

Acknowledgements

We thank the conveners and the participants of the EGU Galileo conference “Exploring new frontiers in fluid processes in subduction zones” for constructive discussions. We also thank Ulrich Linden for the technical support.

Financial support

This work was supported by the Swiss National Science Foundation [Project N. 200021_166280].

https://doi.org/10.5194/se-2019-140
Preprint. Discussion started: 23 September 2019

REFERENCES

Abers, G. A., van Keken, P. E., Kneller, E. A., Ferris, A. and Stachnik, J. C.: The thermal structure of subduction zones constrained by seismic imaging: Implications for slab dehydration and wedge flow, Earth and Planetary Science Letters, 241(3–4), 387–397, 2006.

Airaghi, L., Lanari, P., de Sigoyer, J. and Guillot, S.: Microstructural vs compositional preservation and pseudomorphic replacement of muscovite in deformed metapelites from the Longmen Shan (Sichuan, China), Lithos, 282, 262–280, 2017.

Albarède, F.: The survival of mantle geochemical heterogeneities, Washington DC American Geophysical Union Geophysical Monograph Series, 160, 27–46, 2005.

Alt, J. C., Muehlenbachs, K. and Honnorez, J.: An oxygen isotopic profile through the upper kilometer of the oceanic crust, DSDP Hole 504B, Earth and Planetary Science Letters, 80(3), 217–229, doi:10.1016/0012-821X(86)90106-8, 1986.

Auer, S., Bindeman, I., Wallace, P., Ponomareva, V. and Portnyagin, M.: The origin of hydrous, high-$\delta^{18}O$ voluminous volcanism: diverse oxygen isotope values and high magmatic water contents within the volcanic record of Klyuchevskoy volcano, Kamchatka, Russia, Contributions to Mineralogy and Petrology, 157(2), 209, 2009.

Barnes, J. D. and Straub, S. M.: Chorine stable isotope variations in Izu Bonin tephra: implications for serpentinite subduction, Chemical Geology, 272(1), 62–74, 2010.

Barnicoat, A. C. and Cartwright, I.: Focused fluid flow during subduction: oxygen isotope data from high-pressure ophiolites of the western Alps, Earth and Planetary Science Letters, 132(1–4), 53–61, 1995.

Baumgartner, L. P. and Rumble, D.: Transport of stable isotopes: I: Development of a kinetic continuum theory for stable isotope transport, Contributions to Mineralogy and Petrology, 98(4), 417–430, 1988.

Baumgartner, L. P. and Valley, J. W.: Stable isotope transport and contact metamorphic fluid flow, Reviews in Mineralogy and Geochemistry, 43(1), 415–467, 2001.

Baxter, E. F. and Caddick, M. J.: Garnet growth as a proxy for progressive subduction zone dehydration, Geology, 41(6), 643–646, 2013.

Bebout, G. E. and Penniston-Dorland, S. C.: Fluid and mass transfer at subduction interfaces—The field metamorphic record, Lithos, 240, 228–258, 2016.

Bebout, G. E., Agard, P., Kobayashi, K., Moriguti, T. and Nakamura, E.: Devolatilization history and trace element mobility in deeply subducted sedimentary rocks: Evidence from Western Alps HP/UHP suites, Chemical Geology, 342, 1–20, 2013.

Bostock, M. G., Hyndman, R. D., Rondenay, S. and Peacock, S. M.: An inverted continental Moho and serpentinization of the forearc mantle, Nature, 417(6888), 536, 2002.

Bowman, J. R., Willett, S. D. and Cook, S. J.: Oxygen isotopic transport and exchange during fluid flow: One-dimensional models and applications, American Journal of Science;(United States), 294(1), 1994.

Bulle, F., Rubatto, D., Ruggieri, G., Luisier, C., Villa, I. M. and Baumgartner, L.: Episodic hydrothermal alteration recorded by microscale oxygen isotope analysis of white mica in the Larderello-Travale Geothermal Field, Italy, Chemical Geology, 119288, 2019.

Caddick, M. J., Konopásek, J. and Thompson, A. B.: Preservation of garnet growth zoning and the duration of prograde metamorphism, Journal of Petrology, 51(11), 2327–2347, 2010.

de Capitani, C. and Brown, T. H.: The computation of chemical equilibrium in complex systems containing non-ideal solutions, Geochimica et Cosmochimica Acta, 51(10), 2639–2652, 1987.

de Capitani, C. and Petrakakis, K.: The computation of equilibrium assemblage diagrams with Theriak/Domino software, American Mineralogist, 95(7), 1006–1016, 2010.

Cartwright, I. and Barnicoat, A. C.: Stable isotope geochemistry of Alpine ophiolites: a window to ocean-floor hydrothermal alteration and constraints on fluid–rock interaction during high-pressure metamorphism, International Journal of Earth Sciences, 88(2), 219–235, 1999.

Cartwright, I. and Barnicoat, A. C.: Geochemical and stable isotope resetting in shear zones from Täschalp: constraints on fluid flow during exhumation in the Western Alps, Journal of Metamorphic Geology, 21(2), 143–161, 2003.

Cook-Kollars, J., Bebout, G. E., Collins, N. C., Angiboust, S. and Agard, P.: Subduction zone metamorphic pathway for deep carbon cycling: I. Evidence from HP/UHP metasedimentary rocks, Italian Alps., Chemical Geology, 386, 31–48, 2014.

Diener, J. F. A., Powell, R., White, R. W. and Holland, T. J. B.: A new thermodynamic model for clino-and orthoamphiboles in the system Na2O–CaO–FeO–MgO–Al2O3–SiO2–H2O–O, Journal of Metamorphic Geology, 25(6), 631–656, 2007.

Dorendorf, F., Wiechert, U. and Wörner, G.: Hydrated sub-arc mantle: a source for the Kluchevskoy volcano, Kamchatka/Russia, Earth and Planetary Science Letters, 175(1), 69–86, 2000.

Dubacq, B., Vidal, O. and De Andrade, V.: Dehydration of dioctahedral aluminous phyllosilicates: thermodynamic modelling and implications for thermobarometric estimates, Contributions to Mineralogy and Petrology, 159(2), 159, 2010.

Eiler, J. M.: Oxygen isotope variations of basaltic lavas and upper mantle rocks, Reviews in mineralogy and geochemistry, 43(1), 319–364, 2001.

Eiler, J. M., Farley, K. A., Valley, J. W., Hauri, E., Craig, H., Hart, S. R. and Stolper, E. M.: Oxygen isotope variations in ocean island basalt phenocrysts, Geochimica et Cosmochimica Acta, 61(11), 2281–2293, 1997.

Eiler, J. M., McInnes, B., Valley, J. W., Graham, C. M. and Stolper, E. M.: Oxygen isotope evidence for slab-derived fluids in the sub-arc mantle, Nature, 393(6687), 777, 1998.

Engi, M., Giuntoli, F., Lanari, P., Burn, M., Kunz, B. and Bouvier, A.-S.: Pervasive Eclogitization Due to Brittle Deformation and Rehydration of Subducted Basement: Effects on Continental Recycling?, Geochemistry, Geophysics, Geosystems, 19(3), 865–881, 2018.

https://doi.org/10.5194/se-2019-140
Preprint. Discussion started: 23 September 2019

606 Errico, J. C., Barnes, J. D., Strickland, A. and Valley, J. W.: Oxygen isotope zoning in garnets from Franciscan eclogite blocks:
607 evidence for rock–buffered fluid interaction in the mantle wedge, Contributions to Mineralogy and Petrology, 166(4), 1161–1176,
608 2013.
609 Evans, T. P.: A method for calculating effective bulk composition modification due to crystal fractionation in garnet-bearing
610 schist: implications for isopleth thermobarometry, Journal of Metamorphic Geology, 22(6), 547–557, 2004.
611 Ferry, J. t and Spear, F. S.: Experimental calibration of the partitioning of Fe and Mg between biotite and garnet, Contributions to
612 mineralogy and petrology, 66(2), 113–117, 1978.
613 Frey, M., Capitani, C. de and Liou, J. G.: A new petrogenetic grid for low-grade metabasites, Journal of Metamorphic Geology,
614 9(4), 497–509, 1991.
615 Früh-Green, G. L., Scambelluri, M. and Vallis, F.: O–H isotope ratios of high pressure ultramafic rocks: implications for fluid
616 sources and mobility in the subducted hydrous mantle, Contributions to Mineralogy and Petrology, 141(2), 145–159, 2001.
617 Gale, A., Dalton, C. A., Langmuir, C. H., Su, Y. and Schilling, J.-G.: The mean composition of ocean ridge basalts, Geochemistry,
618 Geophysics, Geosystems, 14(3), 489–518, 2013.
619 Gerdes, M. L., Baumgartner, L. P., Person, M. and Rumble, D.: One-and two-dimensional models of fluid flow and stable isotope
620 exchange at an outcrop in the Adamello contact aureole, Southern Alps, Italy, American Mineralogist, 80(9–10), 1004–1019,
621 1995a.
622 Gerdes, M. L., Baumgartner, L. P. and Person, M.: Stochastic permeability models of fluid flow during contact metamorphism,
623 Geology, 23(10), 945–948, 1995b.
624 Gerya, T. V., Stöckhert, B. and Perchuk, A. L.: Exhumation of high-pressure metamorphic rocks in a subduction channel: A
625 numerical simulation, Tectonics, 21(6), 6–1, 2002.
626 Giuntoli, F., Lanari, P. and Engi, M.: Deeply subducted continental fragments-Part 1: Fracturing, dissolution-precipitation, and
627 diffusion processes recorded by garnet textures of the central Sesia Zone (western Italian Alps), Solid Earth, 9(1), 167–167, 2018.
628 Gregory, R. T. and Taylor Jr, H. P.: An oxygen isotope profile in a section of Cretaceous oceanic crust, Samail ophiolite, Oman:
629 Evidence for $\delta^{18}O$ buffering of the oceans by deep (> 5 km) seawater-hydrothermal circulation at mid-ocean ridges, Journal of
630 Geophysical Research: Solid Earth, 86(B4), 2737–2755, 1981.
631 Hacker, B. R.: H2O subduction beyond arcs, Geochemistry, Geophysics, Geosystems, 9(3), 2008.
632 Hermann, J., Müntener, O. and Scambelluri, M.: The importance of serpentinite mylonites for subduction and exhumation of
633 oceanic crust, Tectonophysics, 327(3–4), 225–238, 2000.
634 Hernández-Uribe, D. and Palin, R. M.: A revised petrological model for subducted oceanic crust: insights from phase equilibrium
635 modelling, Journal of Metamorphic Geology, 2019.
636 Heuret, A. and Lallemand, S.: Plate motions, slab dynamics and back-arc deformation, Physics of the Earth and Planetary
637 Interiors, 149(1–2), 31–51, 2005.
638 Higashino, F., Rubatto, D., Kawakami, T., Bouvier, A.-S. and Baumgartner, L. P.: Oxygen isotope speedometry in granulite facies
639 garnet recording fluid/melt–rock interaction (Sør Rondane Mountains, East Antarctica), Journal of Metamorphic Geology, 2018.
640 Hirauchi, K. and Katayama, I.: Rheological contrast between serpentine species and implications for slab–mantle wedge
641 decoupling, Tectonophysics, 608, 545–551, 2013.
642 Hoefs, J.: Stable isotope geochemistry, Springer, Berlin., 1997.
643 Holland, T. and Powell, R.: Thermodynamics of order-disorder in minerals; II, Symmetric formalism applied to solid solutions,
644 American Mineralogist, 81(11–12), 1425–1437, 1996.
645 Holland, T. and Powell, R.: Activity–composition relations for phases in petrological calculations: an asymmetric multicomponent
646 formulation, Contributions to Mineralogy and Petrology, 145(4), 492–501, 2003.
647 Holland, T., Baker, J. and Powell, R.: Mixing properties and activity-composition relationships of chlorites in the system MgO-
648 FeO-Al2O3-SiO2-H2O, European Journal of Mineralogy, 395–406, 1998.
649 Holland, T. J. B. and Powell, R.: An internally consistent thermodynamic data set for phases of petrological interest, Journal of
650 metamorphic Geology, 16(3), 309–343, 1998.
651 Iwamori, H.: Transportation of H_2O and melting in subduction zones, Earth and Planetary Science Letters, 160(1–2), 65–80, 1998.
652 John, T., Scambelluri, M., Frische, M., Barnes, J. D. and Bach, W.: Dehydration of subducting serpentinite: implications for
653 halogen mobility in subduction zones and the deep halogen cycle, Earth and Planetary Science Letters, 308(1–2), 65–76, 2011.
654 Kerrick, D. M. and Connolly, J. A. D.: Metamorphic devolatilization of subducted marine sediments and the transport of volatiles
655 into the Earth's mantle, Nature, 411(6835), 293, 2001.
656 Kohn, M. J.: Modeling of prograde mineral $\delta^{18}O$ changes in metamorphic systems, Contributions to Mineralogy and Petrology,
657 113(2), 249–261, 1993.
658 Konrad-Schmolke, M., O'Brien, P. J., de Capitani, C. and Carswell, D. A.: Garnet growth at high-and ultra-high pressure
659 conditions and the effect of element fractionation on mineral modes and composition, Lithos, 103(3–4), 309–332, 2008.
660 Kuhn, B. K., Reusser, E., Powell, R. and Günther, D.: Metamorphic evolution of calc-schists in the Central Alps, Switzerland,
661 Schweizerische mineralogische und petrographische Mitteilungen, 85(2–3), 175–190, 2005.
662 Lanari, P. and Duesterhoeft, E.: Modeling Metamorphic Rocks Using Equilibrium Thermodynamics and Internally Consistent
663 Databases: Past Achievements, Problems and Perspectives, Journal of Petrology, 60(1), 19–56, doi:10.1093/petrology/egy105,
664 2018.
665 Lanari, P. and Engi, M.: Local bulk composition effects on metamorphic mineral assemblages, Reviews in Mineralogy and
666 Geochemistry, 83(1), 55–102, 2017.
667 Lanari, P., Giuntoli, F., Loury, C., Burn, M. and Engi, M.: An inverse modeling approach to obtain P–T conditions of
668 metamorphic stages involving garnet growth and resorption, European Journal of Mineralogy, 29(2), 181–199, 2017.

https://doi.org/10.5194/se-2019-140
Preprint. Discussion started: 23 September 2019

669 Laurent, V., Lanari, P., Naïr, I., Augier, R., Lahfid, A. and Jolivet, L.: Exhumation of eclogite and blueschist (Cyclades, Greece):
670 Pressure–temperature evolution determined by thermobarometry and garnet equilibrium modelling, Journal of Metamorphic
671 Geology, 36(6), 769–798, 2018.
672 Liou, J. G., Tsujimori, T., Zhang, R. Y., Katayama, I. and Maruyama, S.: Global UHP metamorphism and continental
673 subduction/collision: the Himalayan model, International Geology Review, 46(1), 1–27, 2004.
674 Manning, C. E.: The chemistry of subduction-zone fluids, Earth and Planetary Science Letters, 223(1–2), 1–16, 2004.
675 Martin, L. A., Rubatto, D., Crépisson, C., Hermann, J., Putlitz, B. and Vitale-Brovarone, A.: Garnet oxygen analysis by SHRIMP-
676 SI: Matrix corrections and application to high-pressure metasomatic rocks from Alpine Corsica, Chemical geology, 374, 25–36,
677 2014.
678 Mattey, D., Lowry, D. and Macpherson, C.: Oxygen isotope composition of mantle peridotite, Earth and Planetary Science
679 Letters, 128(3–4), 231–241, 1994.
680 Mével, C.: Serpentinization of abyssal peridotites at mid-ocean ridges, Comptes Rendus Geoscience, 335(10–11), 825–852, 2003.
681 Miller, J. A. and Cartwright, I.: Distinguishing between seafloor alteration and fluid flow during subduction using stable isotope
682 geochemistry: examples from Tethyan ophiolites in the Western Alps - Miller - 2000 - Journal of Metamorphic Geology - Wiley
683 Online Library, Journal of Metamorphic Geology, 18(5), 467–482, 2000.
684 Miller, J. A., Cartwright, I., Buick, I. S. and Barnicoat, A. C.: An O-isotope profile through the HP–LT Corsican ophiolite, France
685 and its implications for fluid flow during subduction, Chemical Geology, 178(1–4), 43–69, 2001.
686 Muehlenbachs, K. and Clayton, R. N.: Oxygen isotope studies of fresh and weathered submarine basalts, Canadian Journal of
687 Earth Sciences, 9(2), 172–184, 1972.
688 Nakakuki, T. and Mura, E.: Dynamics of slab rollback and induced back-arc basin formation, Earth and Planetary Science Letters,
689 361, 287–297, 2013.
690 O'Neil, J. R. and Taylor, H. P.: The oxygen isotope and cation exchange chemistry of feldspars, American Mineralogist, 52,
691 1414–1437, 1967.
692 Padrón-Navarta, J. A., Hermann, J., Garrido, C. J., Sánchez-Vizcaíno, V. L. and Gómez-Pugnaire, M. T.: An experimental
693 investigation of antigorite dehydration in natural silica-enriched serpentinite, Contributions to Mineralogy and Petrology, 159(1),
694 25, 2010.
695 Padrón-Navarta, J. A., Sánchez-Vizcaíno, V. L., Hermann, J., Connolly, J. A., Garrido, C. J., Gómez-Pugnaire, M. T. and
696 Marchesi, C.: Tschermak's substitution in antigorite and consequences for phase relations and water liberation in high-grade
697 serpentinites, Lithos, 178, 186–196, 2013.
698 Page, F. Z., Kita, N. T. and Valley, J. W.: Ion microprobe analysis of oxygen isotopes in garnets of complex chemistry, Chemical
699 Geology, 270(1–4), 9–19, 2010.
700 Page, F. Z., Essene, E. J., Mukasa, S. B. and Valley, J. W.: A garnet–zircon oxygen isotope record of subduction and exhumation
701 fluids from the Franciscan Complex, California, Journal of Petrology, 55(1), 103–131, 2013.
702 Page, F. Z., Cameron, E. M., Flood, C. M., Dobbins, J. W., Spicuzza, M. J., Kitajima, K., Strickland, A., Ushikubo, T., Mattinson,
703 C. G. and Valley, J. W.: Extreme oxygen isotope zoning in garnet and zircon from a metachert block in mélange reveals
704 metasomatism at the peak of subduction metamorphism, Geology, 47(7), 655–658, 2019.
705 Parra, T., Vidal, O. and Agard, P.: A thermodynamic model for Fe–Mg dioctahedral K white micas using data from phase-
706 equilibrium experiments and natural pelitic assemblages, Contributions to Mineralogy and Petrology, 143(6), 706–732, 2002.
707 Peacock, S. A.: Fluid processes in subduction zones, Science, 248(4953), 329–337, 1990.
708 Peacock, S. M.: The importance of blueschist→ eclogite dehydration reactions in subducting oceanic crust, Geological Society of
709 America Bulletin, 105(5), 684–694, 1993.
710 Penniston-Dorland, S. C., Kohn, M. J. and Manning, C. E.: The global range of subduction zone thermal structures from exhumed
711 blueschists and eclogites: Rocks are hotter than models, Earth and Planetary Science Letters, 428, 243–254, 2015.
712 Plank, T.: The chemical composition of subducting sediments, Treatise on geochemistry, 4, 607–629, 2014.
713 Plank, T. and Langmuir, C. H.: The chemical composition of subducting sediment and its consequences for the crust and mantle,
714 Chemical geology, 145(3), 325–394, 1998.
715 Poli, S. and Schmidt, M. W.: Petrology of subducted slabs, Annual Review of Earth and Planetary Sciences, 30(1), 207–235,
716 2002.
717 Powell, R. and Holland, T. J. B.: On thermobarometry, Journal of Metamorphic Geology, 26(2), 155–179, 2008.
718 Putlitz, B., Matthews, A. and Valley, J. W.: Oxygen and hydrogen isotope study of high-pressure metagabbros and metabasalts
719 (Cyclades, Greece): implications for the subduction of oceanic crust, Contributions to Mineralogy and Petrology, 138(2), 114–
720 126, 2000.
721 Rubatto, D. and Angiboust, S.: Oxygen isotope record of oceanic and high-pressure metasomatism: a P–T–time–fluid path for the
722 Monviso eclogites (Italy), Contributions to mineralogy and petrology, 170(5–6), 44, 2015.
723 Rumble, D.: Stable isotope fractionation during metamorphic devolatilization reactions, Reviews in Mineralogy and
724 Geochemistry, 10(1), 327–353, 1982.
725 Russell, A. K., Kitajima, K., Strickland, A., Medaris, L. G., Schulze, D. J. and Valley, J. W.: Eclogite-facies fluid infiltration:
726 constraints from $\delta^{18}O$ zoning in garnet, Contributions to Mineralogy and Petrology, 165(1), 103–116, 2013.
727 Scambelluri, M. and Philippot, P.: Deep fluids in subduction zones, Lithos, 55(1–4), 213–227, 2001.
728 Scambelluri, M., Fiebig, J., Malaspina, N., Müntener, O. and Pettke, T.: Serpentinite subduction: implications for fluid processes
729 and trace-element recycling, International Geology Review, 46(7), 595–613, 2004.
730 Schmidt, M. W. and Poli, S.: The stability of lawsonite and zoisite at high pressures: Experiments in CASH to 92 kbar and
731 implications for the presence of hydrous phases in subducted lithosphere, Earth and Planetary Science Letters, 124(1–4), 105–118,
732 1994.
733 Sharp, Z.: Principles of stable isotope geochemistry, 2017.

https://doi.org/10.5194/se-2019-140
Preprint. Discussion started: 23 September 2019

Sharp, Z. D. and Barnes, J. D.: Water-soluble chlorides in massive seafloor serpentinites: a source of chloride in subduction zones, Earth and Planetary Science Letters, 226(1–2), 243–254, 2004.

Siron, G., Baumgartner, L., Bouvier, A.-S., Putlitz, B. and Vennemann, T.: Biotite reference materials for secondary ion mass spectrometry $^{18}O/^{16}O$ measurements, Geostandards and Geoanalytical Research, 41(2), 243–253, 2017.

Spandler, C. and Hermann, J.: High-pressure veins in eclogite from New Caledonia; Implications for fluid migration and seismic activity in subduction zones, Geochimica et Cosmochimica Acta Supplement, 69, A664, 2005.

Spear, F. S.: Metamorphic fractional crystallization and internal metasomatism by diffusional homogenization of zoned garnets, Contributions to Mineralogy and Petrology, 99(4), 507–517, 1988.

Spear, F. S., Pattison, D. R. M. and Cheney, J. T.: The metamorphosis of metamorphic petrology, in The Web of Geological Sciences: Advances, Impacts, and Interactions II, Geological Society of America., 2017.

Staudigel, H.: Chemical fluxes from hydrothermal alteration of the oceanic crust, 2014.

Staudigel, H., Plank, T., White, B. and Schmincke, H.-U.: Geochemical fluxes during seafloor alteration of the basaltic upper oceanic crust: DSDP Sites 417 and 418, Subduction: top to bottom, 96, 19–38, 1996.

Stern, R. J.: Subduction zones, Reviews of geophysics, 40(4), 3–1, 2002.

Sun, S.-S. and McDonough, W. F.: Chemical and isotopic systematics of oceanic basalts: implications for mantle composition and processes, Geological Society, London, Special Publications, 42(1), 313–345, 1989.

Syracuse, E. M., van Keken, P. E. and Abers, G. A.: The global range of subduction zone thermal models, Physics of the Earth and Planetary Interiors, 183(1–2), 73–90, 2010.

Tracy, R. J.: Compositional zoning and inclusions in metamorphic minerals., Characterization of Metamorphism through Mineral Equilibria, Review in Mineralogy, 355–397, 1982.

Valley, J.: Stable isotope geochemistry of metamorphic rocks, Rev. Mineral., 16, 445–489, 1986.

Vho, A., Lanari, P. and Rubatto, D.: An internally-consistent database for oxygen isotope fractionation between minerals, Journal of Petrology, *in review*.

Vielzeuf, D., Veschambre, M. and Brunet, F.: Oxygen isotope heterogeneities and diffusion profile in composite metamorphic-magmatic garnets from the Pyrenees, American Mineralogist, 90(2–3), 463–472, 2005a.

Vielzeuf, D., Champenois, M., Valley, J. W., Brunet, F. and Devidal, J. L.: SIMS analyses of oxygen isotopes: matrix effects in Fe–Mg–Ca garnets, Chemical Geology, 223(4), 208–226, 2005b.

Wada, I., Wang, K., He, J. and Hyndman, R. D.: Weakening of the subduction interface and its effects on surface heat flow, slab dehydration, and mantle wedge serpentinization, Journal of Geophysical Research: Solid Earth, 113(B4), 2008.

Walter, M. J.: Melting of garnet peridotite and the origin of komatiite and depleted lithosphere, Journal of Petrology, 39(1), 29–60, 1998.

White, W. M. and Klein, E. M.: Composition of the Oceanic Crust, Treatise on Geochemistry (Second Edition), 2014.

Whitney, D. L. and Evans, B. W.: Abbreviations for names of rock-forming minerals, American mineralogist, 95(1), 185–187, 2010.

Zack, T. and John, T.: An evaluation of reactive fluid flow and trace element mobility in subducting slabs, Chemical Geology, 239(3–4), 199–216, 2007.

https://doi.org/10.5194/se-2019-140
Preprint. Discussion started: 23 September 2019

771 **Table 1.** Bulk compositions used for the simulations.

	SiO_2	TiO_2	Al_2O_3	FeO_T	MnO	MgO	CaO	Na_2O	K_2O	TOTAL	H_2O	CO_2
Normal MORB[1]	50.47	1.68	14.70	10.43	0.18	7.58	11.39	2.79	0.16	99.38	na	na
Normal MORB*	50.47	1.68	14.70	10.43	0.0	7.58	11.39	2.79	0.16	99.20	5.40[§]	0.00
Altered MORB[2]	43.47	1.06	14.74	5.98	0.16	6.32	12.22	1.96	0.53	86.44	7.63	2.80
Altered MORB*	43.47	1.06	14.74	5.98	0.0	6.32	12.22	1.96	0.53	86.28	5.20[§]	2.80
Terrigenous sediment[3]	49.80	0.60	14.70	7.30	2.10	3.10	3.50	3.10	3.60	87.80	10.50	0.00
Terrigenous sediment*	49.80	0.60	14.70	7.30	0.00	3.10	3.50	3.10	3.60	85.70	3.20[§]	0.00
Carbonate Sediment[4]	32.36	0.40	8.78	2.91	0.12	1.45	23.16	1.96	1.66	72.80	8.78	18.20
Carbonate sediment*	32.36	0.40	8.78	2.91	0.00	1.45	23.16	1.96	1.66	72.68	2.10[§]	18.20

772 [1] Gale et al. (2013)
773 [2] Baxter and Caddick (2013) after Staudigel et al. (1996)
774 [3] Mariana clay from Plank and Langmuir (1998)
775 [4] Nanno Ooze from Plank (2014)
776 * used for the thermodynamic modelling
777 [§] water content at saturation at 350 °C and 1.3 GPa. The calculated initial water content is consistent with values from the
778 literature at these conditions (e.g. Poli and Schmidt, 1998; Hacker et al., 2003).
779

https://doi.org/10.5194/se-2019-140
Preprint. Discussion started: 23 September 2019

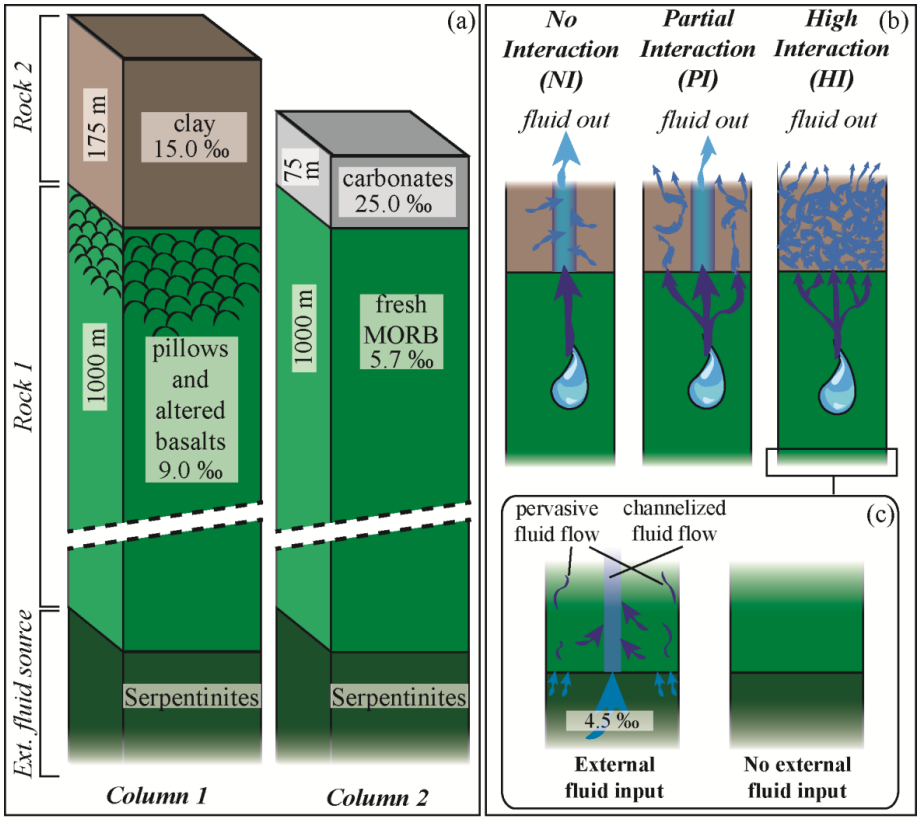

Figure 1. Schematic geometry of the subduction models discussed in the text. The rock column is composed by two rock types (*Rock1* and *Rock2*) that can be infiltrated by an external fluid deriving from a third layer located beneath them. (a) Example columns used in the calculation along the P-T path shown in Fig. 2 to produce the results presented in figures #3-6. See text for details. (b) Schematic representation of the three interaction cases discussed in the text. *No Interaction* case (*NI*): the fluid released by the MORB does not interact with the sedimentary cover. The fluid leaving the system is a mixing of MORB-derived and sediment-derived fluids. *Partial Interaction* case (*PI*): 50% of the MORB-derived fluid does not exchange with the sedimentary cover, and 50% it equilibrates with the sediments. The final fluid released by the system is the mixing between the unmodified mafic fluid and the fluid deriving from the sediment after it equilibrates with 50% of the mafic fluid. *High Interaction* case (*HI*): all the fluid released by the MORB equilibrates with the sediment. The fluid leaving the system exits the sediment. (c) Possible scenario at the base of the column. As a consequence of serpentine breakdown, ultramafic fluid may infiltrate the MORB, exchange with it and affect the fluid infiltrating the sedimentary cover.

https://doi.org/10.5194/se-2019-140
Preprint. Discussion started: 23 September 2019

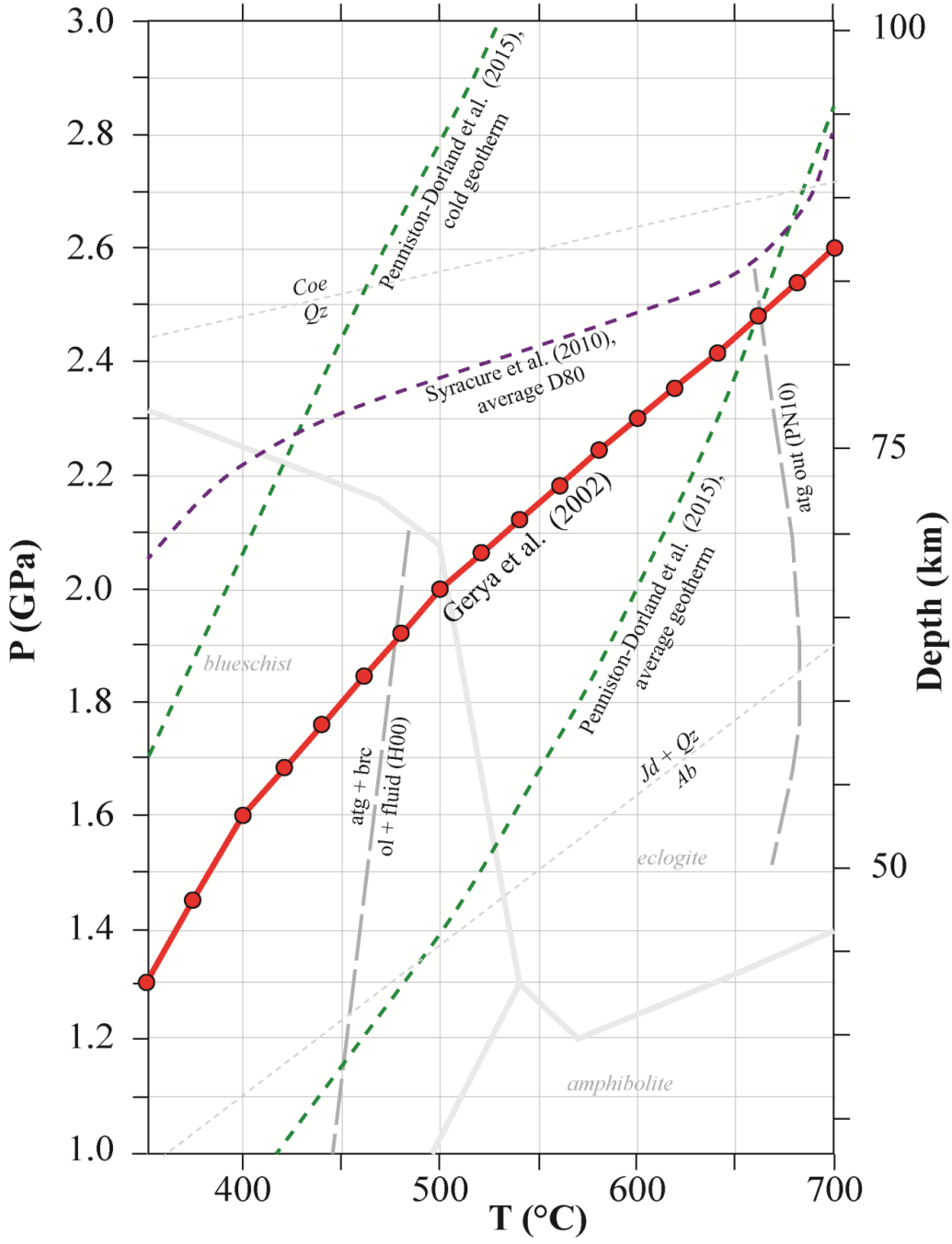

Figure 2. Pressure-Temperature (P-T) diagram showing typical oceanic subduction geotherms and the intermediate geotherm used in the calculation (red line, Gerya et al., 2002). The red spots represent the modelling steps. The average D80 geotherm from Syracuse et al. (2010) as reported by Penniston-Dorland et al. (2015) (purple dotted line) and the average slab-top geotherm from Penniston-Dorland et al. (2015) (green dotted line) are shown for comparison. Metamorphic facies modified from Peacock (1993) and Liou et al. (2004). Serpentine breakdown reactions from Padrón-Navarta et al. (2010) (PN10) and Hermann et al. (2000) (H00). Mineral abbreviations are from Whitney and Evans (2010).

https://doi.org/10.5194/se-2019-140
Preprint. Discussion started: 23 September 2019

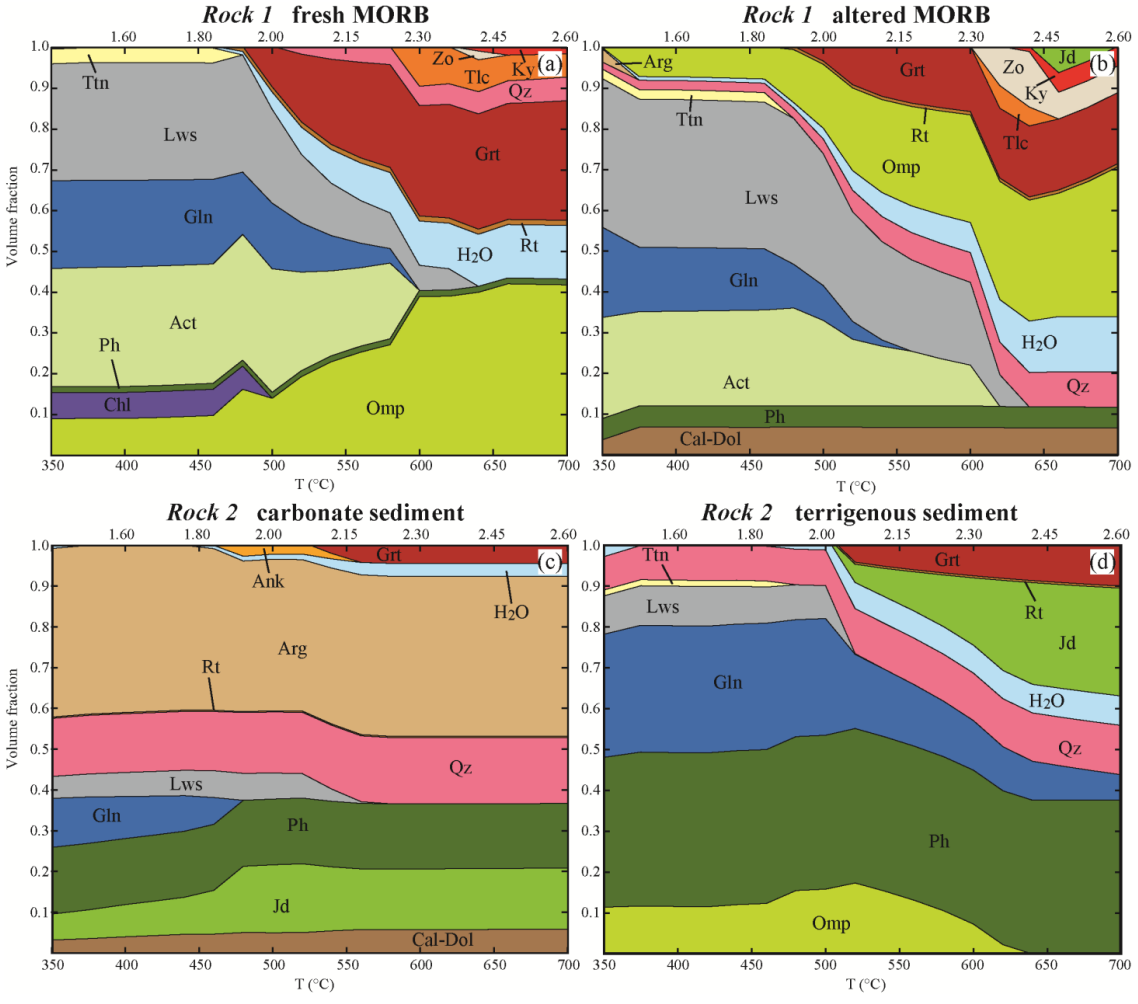

Figure 3. Mode-box diagrams showing the evolution of the mineral assemblages and fluid during subduction of the different rock types along the geotherm shown in Fig. 2. Garnet fractionation is applied to all the lithologies. The volume fraction of garnet shown at each step represents the sum of the fractionated and newly grown garnet. The phase proportions refer to the *NI* case, where the H_2O content is the excess (free) H_2O produced by each rock type evolving independently. The excess water is fractionated at each step and the volume fraction displayed represents the sum of the fractionated and the newly produced water.

https://doi.org/10.5194/se-2019-140
Preprint. Discussion started: 23 September 2019

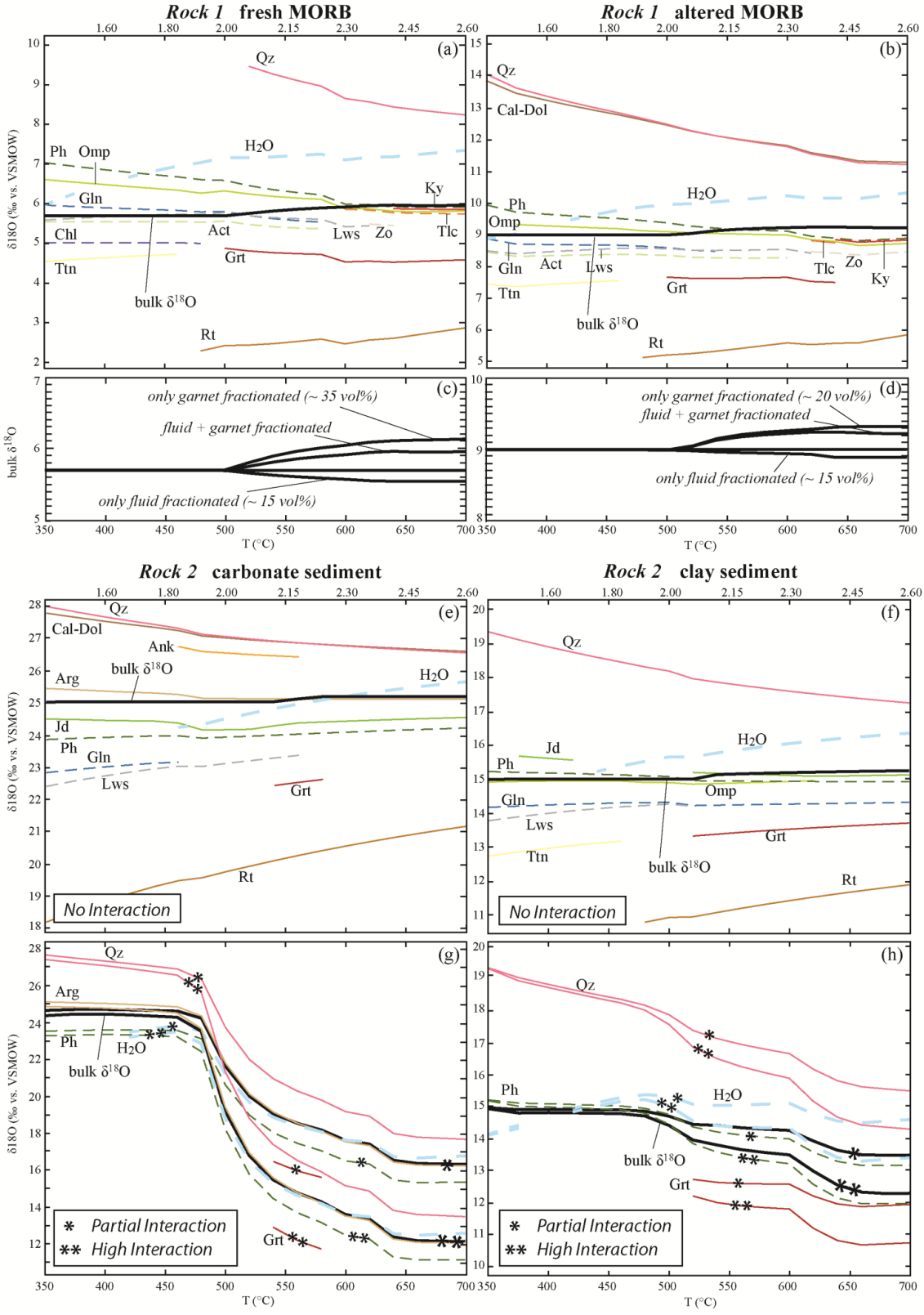

https://doi.org/10.5194/se-2019-140
Preprint. Discussion started: 23 September 2019

809 **Figure 4.** Calculated bulk and mineral $\delta^{18}O$ values along the geotherm shown in Fig. 2. Bulk $\delta^{18}O$: black solid line. Hydrous
810 mineral $\delta^{18}O$: coloured dotted lines. Anhydrous mineral $\delta^{18}O$: coloured solid lines. Released H_2O: thick blue dotted lines. (a, b)
811 Modelled mineral, bulk and released fluid $\delta^{18}O$ values from fresh and altered MORBs considering garnet fractionation and excess
812 fluid loss and in absence of external fluid input. (c, d) Quantification of the effects of garnet fractionation and fluid loss on the
813 bulk $\delta^{18}O$ of the MORB compositions. (e, f) Modelled mineral, bulk and released fluid $\delta^{18}O$ values from carbonate and
814 terrigenous sediments considering garnet fractionation and excess fluid loss and in the absence of external fluid input. (g, h)
815 Modelled $\delta^{18}O$ values from carbonate and terrigenous sediments considering garnet fractionation and excess fluid loss in case of
816 *PI* (*) and *HI* (**). Only bulk, released H_2O and representative mineral $\delta^{18}O$ values are shown for clarity.
817

https://doi.org/10.5194/se-2019-140
Preprint. Discussion started: 23 September 2019

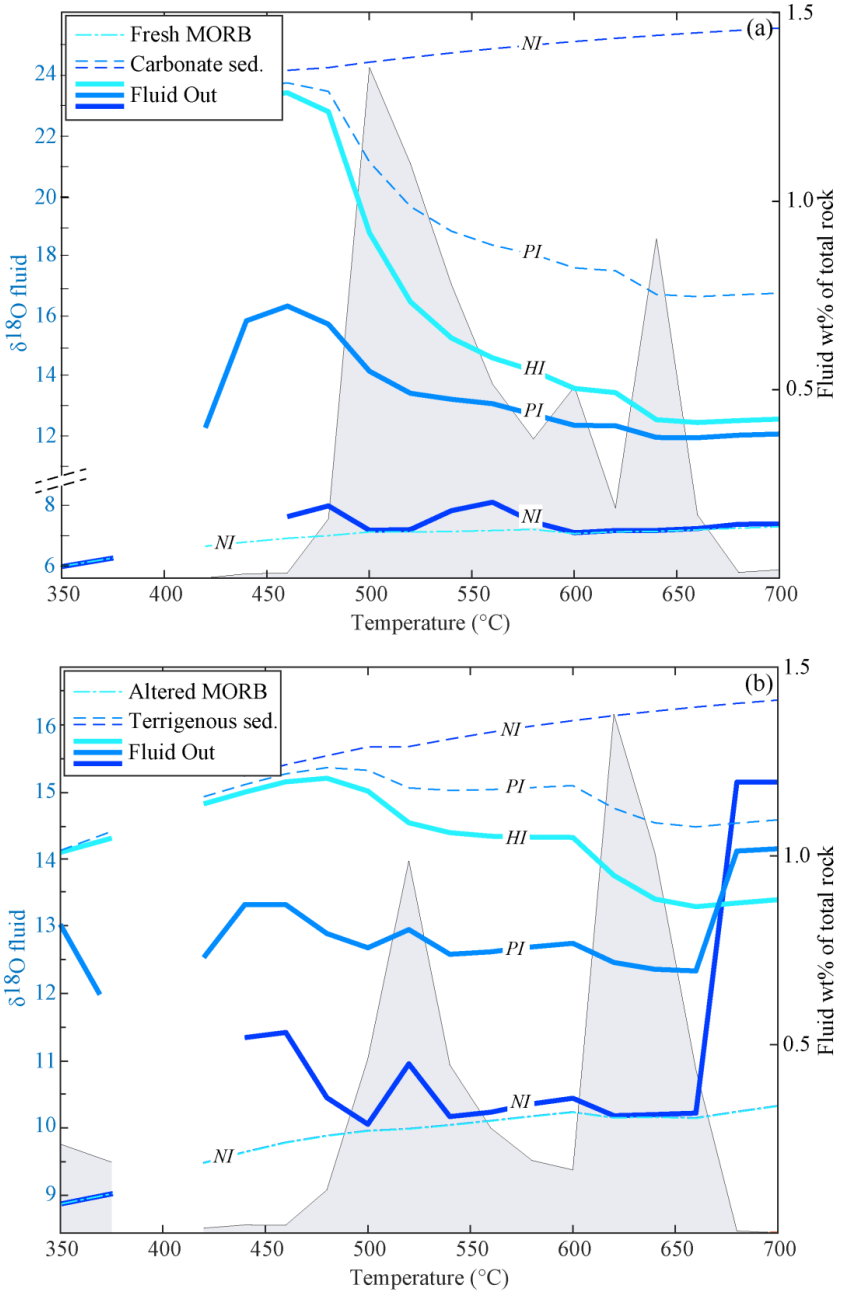

Figure 5. Double plot diagrams showing the oxygen isotope composition of the released fluids (left axis, coloured lines) and the amount (in wt% of the total rock) of the total fluid released by the systems (right axis, grey field) for each interaction case in absence of ultramafic fluid input. (a) Modelled fluid $\delta^{18}O$ values and amount for the system fresh MORB + carbonate sediment. (b) Modelled fluid $\delta^{18}O$ values and amount for the system altered MORB + terrigenous sediment. Dotted lines show the $\delta^{18}O$ values of the fluids released by each rock type, solid lines the $\delta^{18}O$ values of the final fluids released by each system. In case of *HI*, all the MORB-derived fluid infiltrates the sediment. Hence the final fluid released overlaps with the fluid expelled by the sediment and only one line is represented (light blue, marked as *HI*). Because the $\delta^{18}O$ values of the fluids released by the MORB are not affected by the degree of interaction, al three cases are represented by one line (marked as *NI*).

https://doi.org/10.5194/se-2019-140
Preprint. Discussion started: 23 September 2019

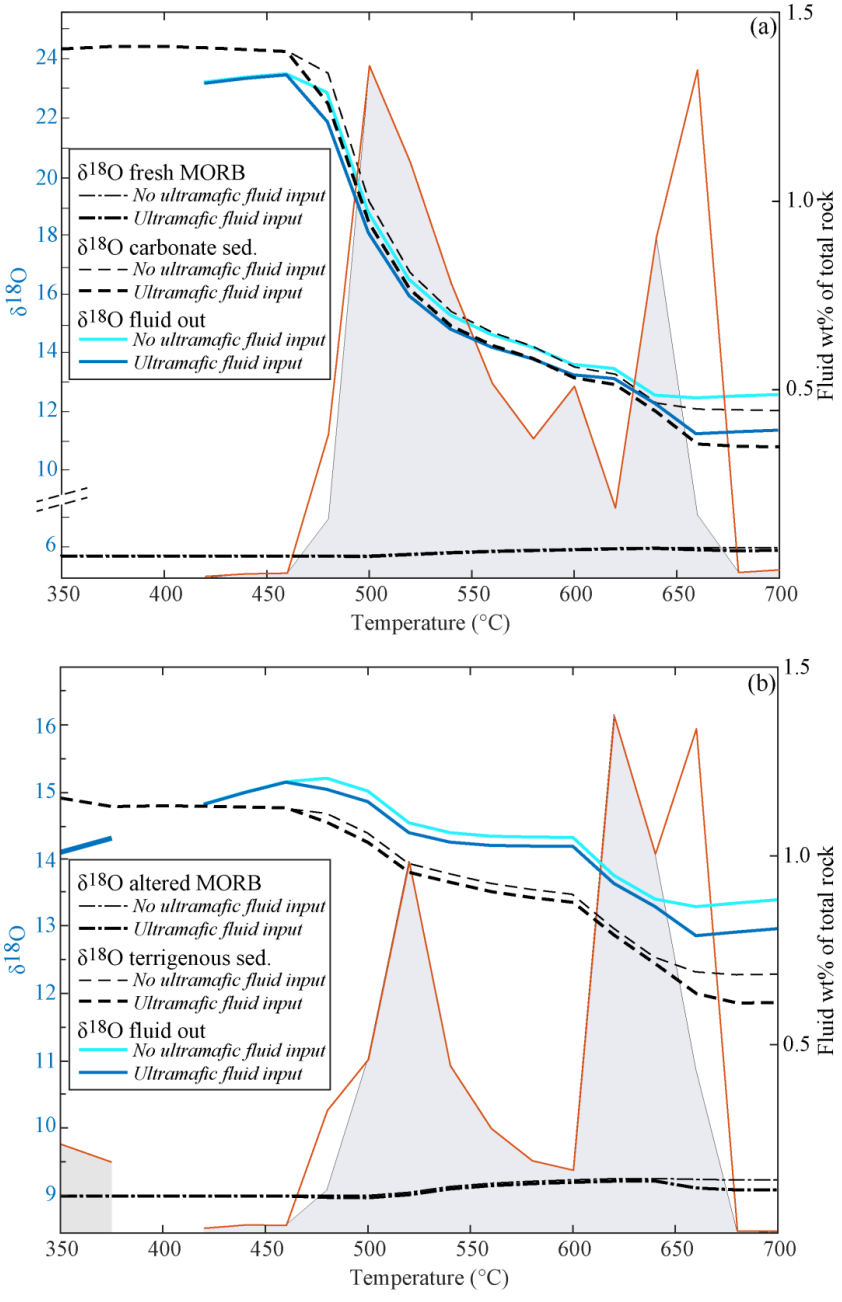

Figure 6. Double plot diagrams showing the effect of the input of the ultramafic fluid deriving from a layer of 150 m of pure serpentine (see text for details) on the $\delta^{18}O$ of the rock types and of the of the total released H_2O (left axis) and on the amount and distribution of the H_2O released by the systems (right axis). All the values are calculated assuming *HI* between the MORBs and the sediments. Black dotted lines represent the bulk $\delta^{18}O$ for the different lithologies and the blue lines the $\delta^{18}O$ of the final fluid released by the systems. The final H_2O released by each system is represented with a red line. The amount and distribution of the final fluids in case of no ultramafic fluid input (grey fields) are shown for comparison. (a) Modelled $\delta^{18}O$ values released fluid amount for the system fresh MORB + carbonate sediment. (b) Modelled $\delta^{18}O$ values released fluid amount for the system altered MORB + terrigenous sediment.

https://doi.org/10.5194/se-2019-140
Preprint. Discussion started: 23 September 2019

836

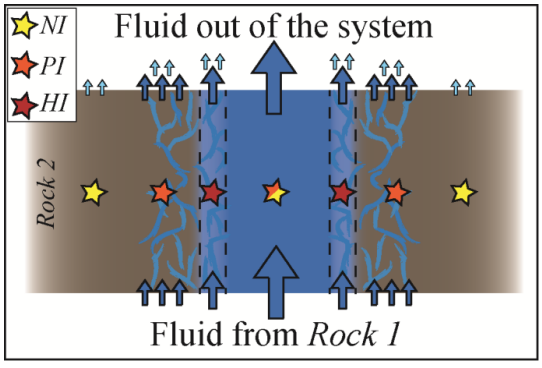

837

838 **Figure 7.** Schematic section of a channelled fluid flow where different degrees of exchange between the fluid and the rock may
839 occur in spatial proximity. From the host rock perspective, the *NI* case describes the distal portion of the rock walls where no fluid
840 infiltrates; the *PI* case the intermediate portion where a limited amount of external fluid is available and the *HI* case the
841 pervasively infiltrated rock proximal to the vein. From the fluid perspective, the *NI* case describes the fluid flow in the centre of
842 the channel, for which the exchange with the rock walls is negligible; the *PI* case the case for which part of the fluid does not react
843 with the wall rock and part equilibrates with it and the *HI* case the situation in which no fluid flows without equilibrating with the
844 host rock.

845

https://doi.org/10.5194/se-2019-140
Preprint. Discussion started: 23 September 2019

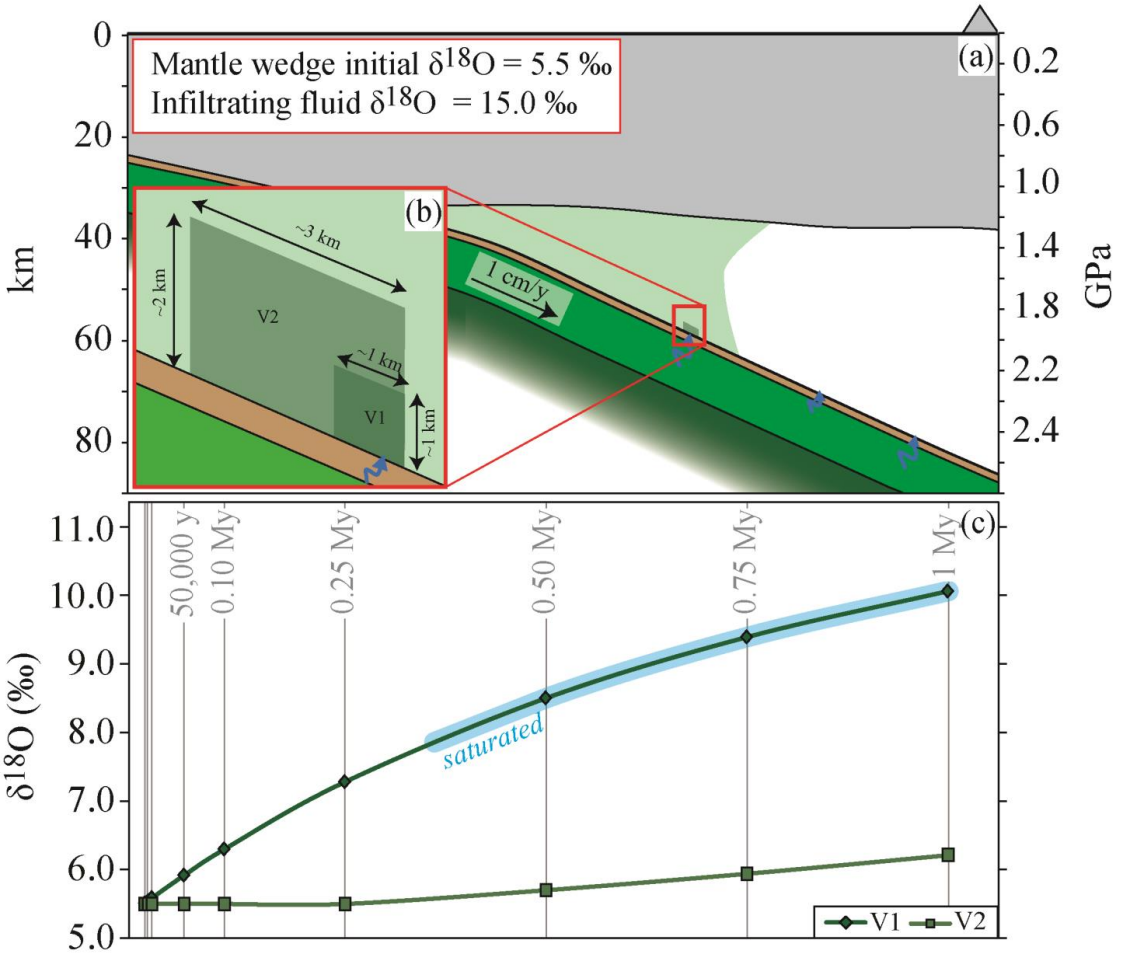

Figure 8. Case model for mantle wedge hydration. (a) Sketch of a subduction zone (modified after Bostock et al., 2002). The subducting slab is composed of altered MORB and terrigenous sediments as shown in Fig. 1a, left column. (b) Geometry of the model. The blue arrow represents slab dehydration at 500 – 520 °C. Abbreviations: V1 represents the volume of mantle rocks at the interface and V2 the surrounding volume (see text for details). (c) Plot of the bulk $\delta^{18}O$ variations of V1 and V2 as consequence of continuous slab dehydration over 1 Myr.